

5-2022

Targeting metabolic adaptations to anti-angiogenic therapy in ovarian cancer

Deanna M. Glassman

Deanna Glassman

Follow this and additional works at: https://digitalcommons.library.tmc.edu/utgsbs_dissertations



Part of the [Biochemical Phenomena, Metabolism, and Nutrition Commons](#), [Obstetrics and Gynecology Commons](#), and the [Therapeutics Commons](#)

Recommended Citation

Glassman, Deanna M. and Glassman, Deanna, "Targeting metabolic adaptations to anti-angiogenic therapy in ovarian cancer" (2022). *The University of Texas MD Anderson Cancer Center UTHealth Graduate School of Biomedical Sciences Dissertations and Theses (Open Access)*. 1156.
https://digitalcommons.library.tmc.edu/utgsbs_dissertations/1156

This Thesis (MS) is brought to you for free and open access by the The University of Texas MD Anderson Cancer Center UTHealth Graduate School of Biomedical Sciences at DigitalCommons@TMC. It has been accepted for inclusion in The University of Texas MD Anderson Cancer Center UTHealth Graduate School of Biomedical Sciences Dissertations and Theses (Open Access) by an authorized administrator of DigitalCommons@TMC. For more information, please contact digitalcommons@library.tmc.edu.

**TARGETING METABOLIC ADAPTATIONS TO ANTI-ANGIOGENIC
THERAPY IN OVARIAN CANCER**

By

Deanna Mae Glassman, MD

APPROVALS:

Anil K. Sood, M.D.
Advisory Professor

Menashe Bar Eli, Ph.D.

Pratip Bhattachayra, Ph.D.

Jinsong Liu, M.D., Ph.D.

Livia Eberlin, M.D.

Scott Kopetz, M.D.

APPROVED:

Dean, The University of Texas
MD Anderson Cancer Center UTHealth Graduate School of Biomedical
Sciences

**TARGETING METABOLIC ADAPTATIONS TO ANTI-ANGIOGENIC
THERAPY IN OVARIAN CANCER**

A

THESIS

Presented to the Faculty of

The University of Texas

MD Anderson Cancer Center UTHealth

Graduate School of Biomedical Sciences

in Partial Fulfillment

of the Requirements

for the Degree of

MASTER OF SCIENCE

by

**Deanna Mae Glassman, MD
Houston, TX**

May, 2022

DEDICATION

To my husband, Tom. Everyday.

ACKNOWLEDGEMENTS

I would like to thank my family who have supported me through my long academic career. They have tolerated my endless travels across the country and stayed with me despite my moving farther away both physically and emotionally with each new training program I enroll in. I am forever grateful to my husband, Tom, who has made sacrifices in his own career, in parenthood, and in his personal life without holding a grudge or developing disdain towards my career goals and aspirations. To my kids, Adler and Riggs, who ironically inspire me to do more and be more for my patients even though it means less time spent with them.

Thank you to Mangala for being my “lab mother” who I could confide in and share stories to break up the day and stresses of basic research. Thank you to Emine and Yuan for sharing the journey of motherhood with me, and for intermittently reaching out to make sure I was “ok.” Thank you to Elaine for always smiling and being so warm and welcoming to me. And thank you to Mark, for showing me how glutaminase works and how to perform a western blot. It may have taken a while to get more than four words out of you—but you led by quiet example and I am truly grateful for that.

Finally, a thank you to Dr. Sood for pushing me to be productive. After attending the first lab meeting over Zoom at the peak of the COVID pandemic, I was convinced that I would never get to the point where I could learn the language of basic science, let alone read Cell papers and actually understand them. Today, I look back on our first conversations about potential projects and I am appreciative of how far all of those projects have come, including this one. Thank you.

TARGETING METABOLIC ADAPTATIONS TO ANTI-ANGIOGENIC THERAPY IN OVARIAN CANCER

Deanna Mae Glassman, M.D.

Advisory Professor: Anil K. Sood, M.D.

ABSTRACT

Background: Ovarian cancer is the most lethal gynecologic malignancy. Despite modest clinical improvements with anti-VEGF antibody (AVA) therapy, adaptive resistance is nearly ubiquitous and additional therapeutic options are limited. A dependence on glutamine metabolism, *via* the enzyme glutaminase (GLS), is a known mechanism of adaptive resistance.

Purpose: To assess the efficacy of a glutaminase inhibitor as a means of exploiting the metabolic vulnerability of glutamine dependence that develops as a result of adaptive resistance to AVA therapy.

Experimental Design: We used a glutaminase inhibitor (GLSi) synthesized at MD Anderson Cancer Center for all *in vitro* and *in vivo* experiments. We first assessed the *in vitro* effect of culturing ovarian cancer cell lines under hypoxic conditions and subsequently evaluated the metabolic adaptations that occurred as a result of this metabolic stress. Following this, we analyzed the effects of GLSi treatment on these cells. We then performed a series of *in vivo* experiments to determine the efficacy of GLSi therapy and the downstream metabolic impact of treatment. Statistical analysis of

all experiments was performed using Student *t* test or Mann-Whitney test, as applicable, with a *p* value < 0.05 considered significant.

Results: Eight ovarian cancer cell lines were screened for glutaminase (GLS) expression with the SKOV3 cell line demonstrating the greatest expression and therefore it was utilized for all *in vivo* experiments. We demonstrated a significant sensitivity of these GLS-expressing cells to GLSi treatment *in vitro*. AVA treatment *in vivo* was associated with an increased abundance of glutamine in tumor tissue. Treatment with a GLSi in this setting led to a reduction in tumor growth and decreased metabolic conversion of pyruvate to lactate as assessed by hyperpolarized magnetic resonance spectroscopy. Furthermore, GLSi therapy initiated after the emergence of AVA resistance restored sensitivity to AVA therapy as evidenced by a reduction in tumor volume and a prolongation of survival of the orthotopic mouse model.

Conclusions: Our analyses indicate that alterations in glutamine metabolism occur in adaptive resistance to AVA therapy and that this can be targeted by GLSi therapy. The combination of AVA and GLSi *in vivo* led to robust anti-tumor responses supporting the inclusion of this combination of therapy in future clinical trials in the setting of AVA resistance.

TABLE OF CONTENTS

APPROVALS:	i
TITLE PAGE	ii
DEDICATION	iii
ACKNOWLEDGEMENTS	iv
ABSTRACT	v
TABLE OF CONTENTS	vii
LIST OF ILLUSTRATIONS	viii
LIST OF TABLES	x
ABBREVIATIONS	xi
BACKGROUND AND INTRODUCTION	1
HYPOTHESIS AND SPECIFIC AIMS	16
RESULTS	30
CONCLUSIONS	75
BIBLIOGRAPHY	76
Permissions	87
Vita	91

LIST OF ILLUSTRATIONS

Figure 1. Percent of cases by stage and five-year relative survival in ovarian cancer patients by stage at diagnosis.	2
Figure 2. Diagram of the numerous metabolic pathways mediated by the VEGF receptor family.....	4
Figure 3. Hypoxia within solid tumors.....	6
Figure 4. Kaplan-Meier curves for two large randomized controlled trials investigating the efficacy of AVA (bevacizumab) in combination with chemotherapy treatment...	8
Figure 5. Metabolic and biosynthetic fates of glutamine.....	12
Figure 6. Kaplan-Meier curve of disease-specific survival as it relates to GLS1 expression.....	14
Figure 7. Working model of the central hypothesis.	17
Figure 8. Metabolic alterations in hypoxia and resulting from AVA therapy.	30
Figure 9. In vivo model of adaptive resistance to AVA therapy.	31
Figure 10. Adaptive resistance to AVA therapy.....	32
Figure 11. Effect of AVA resistance on markers of hypoxia and vascular cell density.	33
Figure 12. Impact plot of adaptive resistance to AVA therapy in an orthotopic murine model of ovarian cancer suggests alterations in purine metabolism.	35
Figure 13. Metabolic alterations in the purine metabolism pathway after adaptive resistance to AVA therapy in an orthotopic murine model of ovarian cancer.	36
Figure 14. Heat map of altered metabolic pathways in murine ovarian cancer model with adaptive resistance to AVA therapy.	37
Figure 15. Heat map of metabolic alterations assessed by DESI-MS in ovarian cancer with adaptive resistance to AVA therapy.....	40
Figure 16. Normalized ion abundance ratio of glutamate to glutamine in AVA-resistance.....	41
Figure 17. DESI-MS ion images of ovarian tumors with adaptive resistance to AVA therapy	42
Figure 18. Effect of HIF-1 α on GLS expression.	44
Figure 19. Baseline GLS expression levels in ovarian cancer and endothelial cells. ..	45

Figure 20. Hypoxia enhances sensitivity to GLS inhibition in both cancer and endothelial cells in vitro.	47
Figure 21. Assessment of angiogenic potential of cells upon culturing with AVA and GLSi in normoxic and hypoxic conditions.	49
Figure 22. Experimental plan to investigate the efficacy of GLSi in vivo.	50
Figure 23. Robust antitumor effect of GLSi combined with AVA as assessed using gross necropsy.	51
Figure 24. Effect of GLSi combined with AVA on tumor burden in an SKOV3ip1 mouse model at time of gross necropsy.	52
Figure 25. Mouse body weight after treatment with AVA, GLSi or combination therapy.	53
Figure 26. Immunohistochemistry analysis of vascular density and cellular proliferation after treatment with AVA, GLSi or combination therapy.	54
Figure 27. Heat map of altered metabolites seen after treatment with AVA and GLSi mono- and combo-therapy.	55
Figure 28. Normalized ion abundance of key metabolites after combination therapy with GLSi and AVA treatment.	57
Figure 29. DESI-MS ion images of ovarian tumors after treatment with either AVA, GLSi, or combination therapy.	60
Figure 30. Detection of GLSi therapy response by HP-MRS.	62
Figure 31. Experimental plan to evaluate if AVA resistance can be restored with GLSi therapy.	63
Figure 32. AVA sensitivity is restored when GLSi therapy is administered after AVA resistance is established.	64
Figure 33. Kaplan-Meier survival curve showing survival advantage with GLSi therapy after AVA resistance is established.	66

LIST OF TABLES

None

ABBREVIATIONS

Listed in alphabetical order:

AVA – Anti-VEGF antibody

BID – twice daily

CT – computerized tomography

DESI-MS – desorption electrospray ionization-mass spectroscopy

FDA – Food and Drug Administration

GLS – glutaminase

GLSi – glutaminase inhibitor

HIF-1 α – Hypoxia inducible factor – 1 alpha

HP-MRS – Hyperpolarized magnetic resonance spectroscopy

IHC – Immunohistochemistry

i.p. – Intraperitoneal

LC-MS – liquid chromatography mass spectroscopy

MRI – magnetic resonance imaging

NCI – National Cancer Institute

ORR – overall response rate

OS – Overall survival

PFS – Progression free survival

SEER – Surveillance, Epidemiology, and End Results program

SPP – Survival post progression

TME – Tumor microenvironment

VEGF – vascular endothelial growth factor

BACKGROUND AND INTRODUCTION

Epidemiology of ovarian cancer

Ovarian cancer most frequently presents as an advanced stage disease making it the most lethal of all gynecologic malignancies, claiming the lives of more than 14,000 women each year.^{1,4} Contributing to the lethality is the fact that the early symptoms of ovarian cancer are subtle and include abdominal bloating, changes in bowel habits, weight gain, and menstrual irregularities.⁵ Given that ovarian cancer is a disease of peri- or post-menopausal women⁶ there is often a misattribution of these associated symptoms to the menopausal transition, or as a manifestation of stress or other benign gastroenterological conditions such as irritable bowel syndrome.⁷ As such, nearly one-fourth (22%) of patients ultimately diagnosed with ovarian cancer receive a diagnosis of a gastroenterological problem in the year preceding the final correct diagnosis.⁷ Generally, more severe symptoms that would prompt a patient to seek an urgent medical evaluation occur only after the disease has become metastatic.⁵ In fact, small retrospective studies have estimated that nearly 90% of women who are diagnosed with ovarian cancer experience one or more diagnostic delays due to the vague nature of their symptoms.⁸ These sorts of diagnostic delays therefore contribute to the increased incidence of advanced stage disease at diagnosis. Unfortunately, the overwhelming majority of patients (>80%) are diagnosed with distant metastatic spread and this translates to a 5-year survival of approximately 30% (Figure 1).¹ Despite these dismal numbers, an under-appreciated fact is that disease prevalence is increasing. Estimates by the Surveillance, Epidemiology, and End Results (SEER) program of the National Cancer Institute (NCI) indicate that the prevalence of ovarian cancer cases in the

United States is approximately 250,000. This represents a 10-fold increase over annualized incidence that has increased over 25% in the last five years.¹ Much of this comes as a result of drugs extending PFS without increasing cure rates. Therefore, new drugs and combinations could have a meaningful impact for women with ovarian cancer.

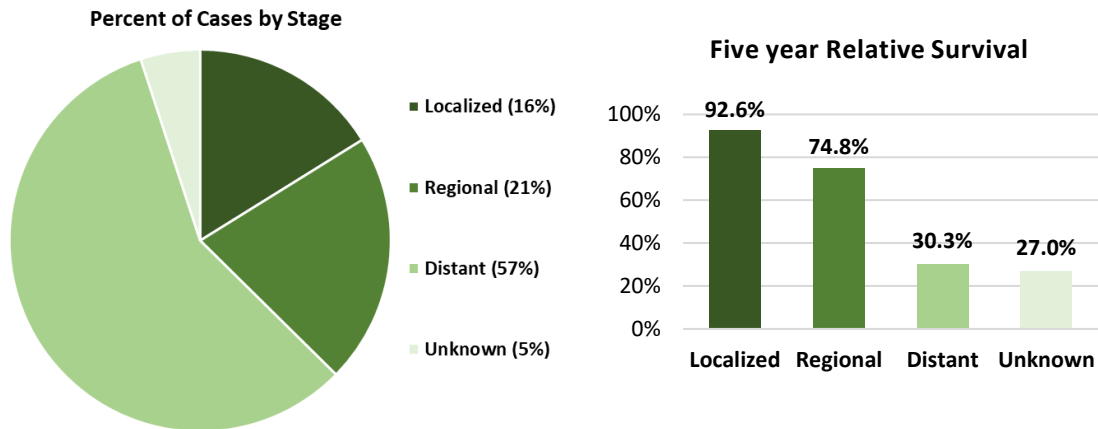


Figure 1. Percent of cases by stage and five-year relative survival in ovarian cancer patients by stage at diagnosis. Figure adapted from *Surveillance, Epidemiology, and End Results (SEER) Program* (www.seer.cancer.gov) SEER*Stat Database: Incidence - SEER Research Data, 9 Registries, Nov 2020 Sub (1975-2018) - Linked To County Attributes - Time Dependent (1990-2018) Income/Rurality, 1969-2019 Counties, National Cancer Institute, DCCPS, Surveillance Research Program, released April 2021, based on the November 2020 submission. *Cancer Stat Facts: Ovarian Cancer. SEER Research Data 2011-2017.* <https://seer.cancer.gov/data/citation.html>. Published 2022. Accessed March 8, 2022.¹

Treatment strategies in ovarian cancer

Once diagnosed, the backbone of treatment for advanced (stage 3-4) ovarian cancer includes tumor reductive surgery aimed at removing all visible disease, followed by platinum-based cytotoxic chemotherapy.⁹ Traditionally, the approach is to use what is called doublet therapy, where treatment is initiated with a combination of carboplatin and paclitaxel; these work by disrupting DNA cross-linkages and altering microtubule stability, respectively.¹⁰ The therapeutic efficacy of this up-front doublet regimen in treating advanced stage ovarian cancer is well established.^{10,11} However, despite initial response rates for first-line treatment ranging from 70-80%, the majority of these women with advanced stage disease will subsequently relapse or progress and require further treatment.^{12,13} Since the mid-1990's, the treatment options for ovarian cancer were simple since there were only a handful of therapeutic agents to choose from.¹² A turning point in therapeutic advances occurred in 2014 when several new classes of drugs, including the targeted agent called bevacizumab, gained approval from the U.S. Food and Drug Administration (FDA).¹⁴

Bevacizumab is a humanized monoclonal antibody against the vascular endothelial growth factor (VEGF) receptor present on endothelial and other cells.^{14,15} This anti-VEGF antibody (AVA) therapy targets one of the established hallmarks of cancer: angiogenesis, or the capability of a tumor to develop new blood vessels.^{16,17} Above and beyond angiogenesis, VEGF is an attractive target for development as a therapeutic strategy because of the relationship that the VEGF receptor has with many well-known metabolic pathways that ultimately impact cell survival, cell migration, and cell proliferation in addition to angiogenesis as highlighted below in Figure 2.¹⁸ Given the significant regulatory role that it plays, it is no surprise that

tumors possess large reservoirs of VEGF and that targeting this with AVA therapy is a rational approach to anti-cancer therapy.¹⁸

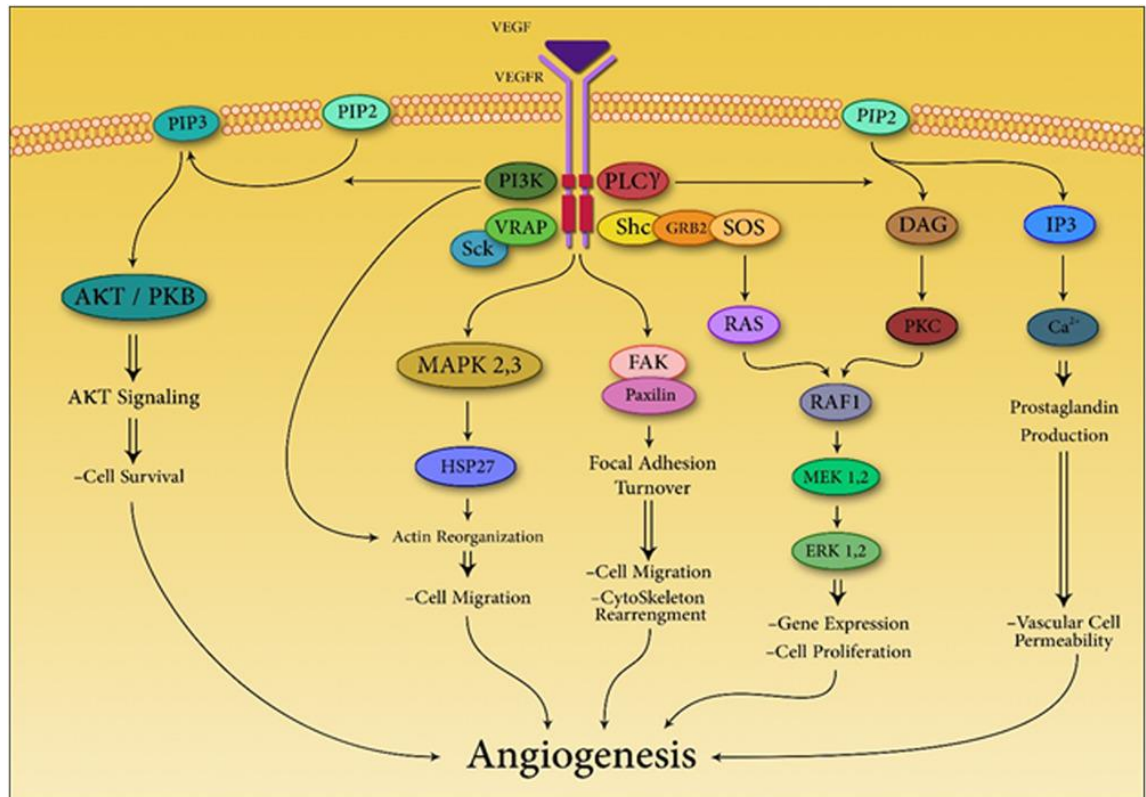


Figure 2. Diagram of the numerous metabolic pathways mediated by the VEGF receptor family. Effects of activation of the VEGF receptor include regulation of pathways involved in cell survival, cell migration, cell proliferation, and vascular permeability via the AKT/PKB, PI3K, MAPK and PIP2 pathways, respectively, before the downstream effect of increased angiogenesis. Figure reprinted with permission. Mahdi A, Darvishi B, Majidzadeh-A K, Salehi M, and Farahmand L. Challenges facing antiangiogenesis therapy: The significant role of hypoxia-inducible factor and MET in development of resistance to anti-vascular endothelial growth factor-targeted therapies. *J Cell Physiol.* 2019;234(5):5655-5663. DOI: 10.1002/jcp.27414.¹⁸

AVA therapy and the impact of hypoxia

Due to the abnormal vasculature inherent in solid tumors during malignant growth, it has been well described that tumors possess hypoxic and even anoxic regions (Figure 3) as a result of the imbalance between tumor proliferation rate and oxygen content.² The increased metabolic activity in proliferative tumors means that the oxygen demand exceeds oxygen supply, therefore leading to this hypoxia.¹⁹ Compared to physiologic oxygen tensions within the parenchyma of normal organs of 20-40%, the oxygen tensions within solid tumors is much lower, estimated to be 1-2%.²⁰ After the additional hypoxic stress imposed by treatment with AVA therapy, these oxygen tension levels are estimated to be even lower than 1%.^{20,21}

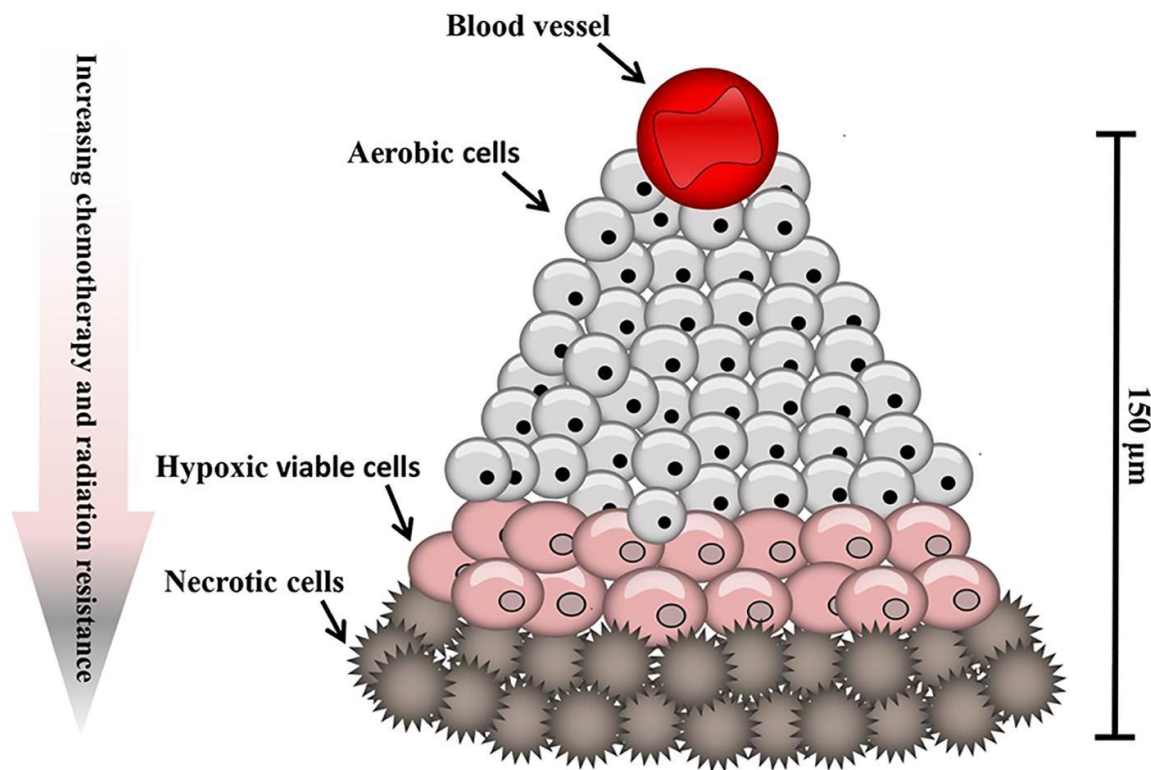


Figure 3. Hypoxia within solid tumors. Tumors possess areas of both hypoxia and necrosis due to the disorganized vasculature leading to an imbalance of available oxygen and nutrient demands and blood supply. Figure reprinted with permission. All *Frontiers* articles from July 2012 onwards are published with open access under the CC-BY Creative Commons attribution license (the current version is CC-BY, version 4.0). The content is free to download, distribute, and adapt for commercial or non-commercial purposes, given appropriate attribution to the original article. Al Tameemi W, Dale TP, Al-Jumaily RMK, and Forsyth NR. Hypoxia-Modified Cancer Cell Metabolism. *Frontiers in cell and developmental biology*. 2019;7:4-4.²

While hypoxia in a normal cell would lead to cell death, hypoxia in tumor cells can induce a selective pressure that breeds resilient cells (Figure 3). This leads to the survival of subpopulations of cells that possess genomic changes enabling them to adapt to the hypoxic stress and maintain adequate nutrition despite the hostile tumor microenvironment (TME).² As described by Hanahan et al. and others, during tumor growth and progression there is an “angiogenic switch” that becomes activated making the normally quiescent process of neovascularization become constitutively activated as a way to thrive despite the lack of oxygen.^{20,22} This leads to continual expansion of new vessels to help meet the high oxygen demand and therefore support ongoing tumor growth and development.²² A number of regulators

of this “switch” have been identified, but targeting VEGF and its receptors has proven most promising because they serve as a rate-limiting factor of the angiogenic function of the tumor cells.²² Therefore, AVA treatment represents not only one of the first targeted agents against angiogenesis but also is the first effective biologically targeted therapy within the realm of ovarian cancer treatment, specifically.¹⁴

Targeting angiogenesis with AVA therapy further increases the relative hypoxia in the TME, starving the tumor of important nutrients for growth and inducing an even greater dependence on hypoxia adaptations.^{17,23} Adding to its efficacy as a targeted therapy, AVA has been found to be potentiated by paclitaxel’s antiangiogenic properties of inhibiting endothelial cell proliferation and migration, and AVA is also known to be synergistic with carboplatin because carboplatin induces VEGF expression in the TME.²⁴ Due to these combined mechanisms, AVA treatment is added to traditional chemotherapy at the time of first recurrence. In this setting, AVA has consistently demonstrated modest improvements in the time to disease recurrence, also known as progression free survival (PFS), across five principal phase III randomized trials of women with advanced stage ovarian cancer.²⁴⁻²⁷ Two of these trials, titled AURELIA and OCEANS, are represented in Figure 4 below and demonstrate that in patients with platinum-resistant and platinum-sensitive disease, there is a 52% and 55% reduction in the risk of progression or death with a PFS benefit of 3.3 and 3.7 months, respectively when AVA therapy (bevacizumab) is combined with traditional chemotherapy.^{25,27}

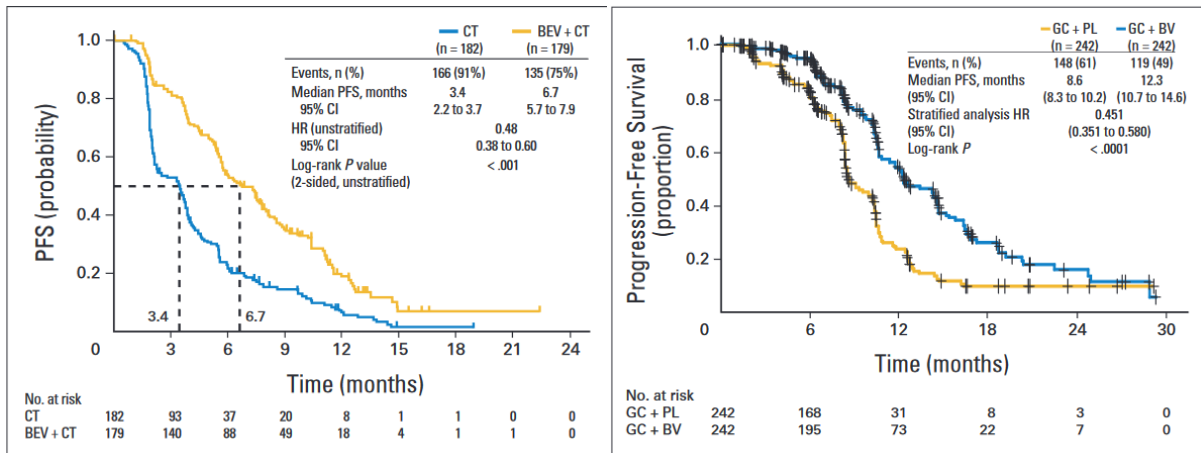


Figure 4. Kaplan-Meier curves for two large randomized controlled trials investigating the efficacy of AVA (bevacizumab) in combination with chemotherapy treatment. (Left) Survival curve demonstrating the progression free survival benefit from bevacizumab of 3.3 months (HR 0.48, $p < 0.001$) from a phase III trial called AURELIA²⁷ which evaluated the combination of bevacizumab and chemotherapy for platinum-resistant recurrent ovarian cancer. CT, chemotherapy; Bev, bevacizumab, HR, hazard ratio. **(Right)** Survival curve representing the progression free survival benefit from bevacizumab of 3.7 months (HR 0.45, $p < 0.0001$) from a phase III trial called OCEANS²⁵ which evaluated the combination of bevacizumab and chemotherapy for platinum-sensitive recurrent ovarian cancer. GC, gemcitabine + carboplatin; BV, bevacizumab; PL, placebo, HR, hazard ratio. Figures reprinted with permission from Pujade-Lauraine E, Hilpert F, Weber B, Reuss A, Poveda A, Kristensen G, Sorio R, Vergote I, Witteveen P, Bamias A, Pereira D, Wimberger P, Oaknin A, Mirza MR, Follana P, Bollag D, Ray-Coquard I. Bevacizumab combined with chemotherapy for platinum-resistant recurrent ovarian cancer: The AURELIA open-label randomized phase III trial. *J Clin Oncol.* 2014;32(13):1302-1308 and Aghajanian C, Blank SV, Goff BA, Judson PL, Teneriello MG, Husain A, Sovak

MA, Jing Yi, Nycum LR. OCEANS: A Randomized, Double-Blind, Placebo-Controlled Phase III Trial of Chemotherapy With or Without Bevacizumab in Patients With Platinum-Sensitive Recurrent Epithelial Ovarian, Primary Peritoneal, or Fallopian Tube Cancer. J Clin Oncol. 2012;30(17):2039-2045. These articles are published with open access under the CC-BY Creative Commons attribution license (the current version is CC-BY, version 4.0). The content is free to download, distribute, and adapt for commercial or non-commercial purposes, given appropriate attribution to the original article.

Beyond this demonstrated efficacy in the relapsed or recurrent setting, there have been additional trials indicating a similar PFS benefit when given as first line treatment, known as the “up-front” setting (i.e. GOG-218 and ICON7 trials).^{26,28} These findings therefore led to AVA therapy with bevacizumab gaining approval by the FDA for use in both the up-front and recurrent disease settings.¹⁴ Practically speaking, this means that nearly all patients with advanced ovarian cancer will be treated with AVA therapy at some point in their care.

Adaptive resistance to AVA therapy in ovarian cancer and the role of glutamine

Unfortunately, despite the modest improvement in PFS as outlined above, a more durable overall survival (OS) benefit from AVA therapy has yet to be recognized in any setting.^{24,29} This is likely due to the emergence of a rapid adaptive resistance within several months of initiating AVA treatment, which thus prevents the achievement of any OS benefit.²⁹ Additionally, the lack of OS benefit may also

be due to the intrinsic limitations of OS as a metric itself. While OS is one of the most frequently utilized endpoints used in drug development, it is not necessarily the most reliable method of determining therapeutic efficacy. A more accurate assessment of drug responses in recurrent disease is the interval of time that patient survives after progression of disease, known as survival post-progression (SPP).³⁰ The longer SPP that a patient has, the less reliable OS is as a metric. Historically, FDA approval of new therapeutic drugs is based on OS, however approvals are increasingly based on PFS or overall response rate (ORR) because of these limitations in OS.

However, despite the limitations of OS, drug resistance in recurrent ovarian cancer translates to the fact that it is almost never cured, with the majority of women spending the duration of their time with relapsed disease (i.e. the SPP interval) switching from one drug to another until the disease again progresses without any further options to treat it. This therefore underscores the importance of deciphering the mechanisms by which tumors develop an adaptive resistance to AVA therapy and a pressing need for more effective treatment strategies to overcome AVA resistance.

In both preclinical and clinical models, blocking the VEGF signaling axis pictured above in Figure 2 results in a metabolic rewiring as a means of maintaining energy supply for tumor growth.¹⁵ One of the adaptations to the hypoxic environment induced by AVA therapy is an upregulation of the expression of a family of hypoxia inducible factors (HIF), namely HIF-1 α and HIF-2 α , which in turn, can lead to an upregulation of compensatory cellular processes that circumvent the inhibition of angiogenesis.¹⁸ These include alternate or parallel pathways of angiogenesis, as well as pathways involved in catabolism and cellular proliferation, erythropoiesis,

apoptosis.³¹ It is therefore plausible that targeting neovascularization with AVA and also simultaneously targeting the associated hypoxic adaptations driven by HIF-1 α could yield improved therapeutic results and potentiate the duration of effect of AVA therapy.²³

Of the known metabolic adaptations that occur in AVA resistance, glucose metabolism has been a central theme of investigation following the discovery of the now well-described Warburg effect, whereby tumors rely on alternative respiration instead of engaging in mitochondrial oxidative phosphorylation to maintain energy for anaplerosis.^{32,33} But beyond glucose metabolism, there has been growing emphasis on the role of alternate nutrients, such as glutamine, which helps to sustain a high level of proliferation even under conditions of hypoxia and glucose deprivation.^{34,35} In fact, some cancer cell types demonstrate a “glutamine dependence” or “glutamine addiction” where they fail to grow or proliferate in the absence of glutamine.³⁶ In preclinical models when tumors are under the hypoxic stress imposed by AVA, part of the metabolic rewiring observed in the TME is an increase in glutamine metabolism (glutaminolysis) as a means to circumvent the reduced capacity for aerobic respiration.²³ This then, represents a possible vulnerability that could be targeted in ovarian cancer.

Glutaminolysis and its significance in ovarian cancer

As demonstrated in Figure 5 below, the downstream effects of glutaminolysis are multifaceted. Glutamine can be utilized as a source of carbon and nitrogen to support biosynthesis and cellular hemostasis but can also serve as a building block for glutathione, a scavenger for reactive oxygen species.^{34,37} Because of this

plurality of glutamine utilization, it is understandable that glutamine dependence has been linked to the level of invasiveness of cancer cells *in vitro* and that glutaminolysis correlates clinically with poor survival.³⁸ The ultimate utilization of glutamine requires its catabolism by the enzyme glutaminase (GLS) into the active metabolite, glutamate, which is subsequently converted to α -ketoglutarate for its use in the Krebs's cycle (Figure 5).³⁹

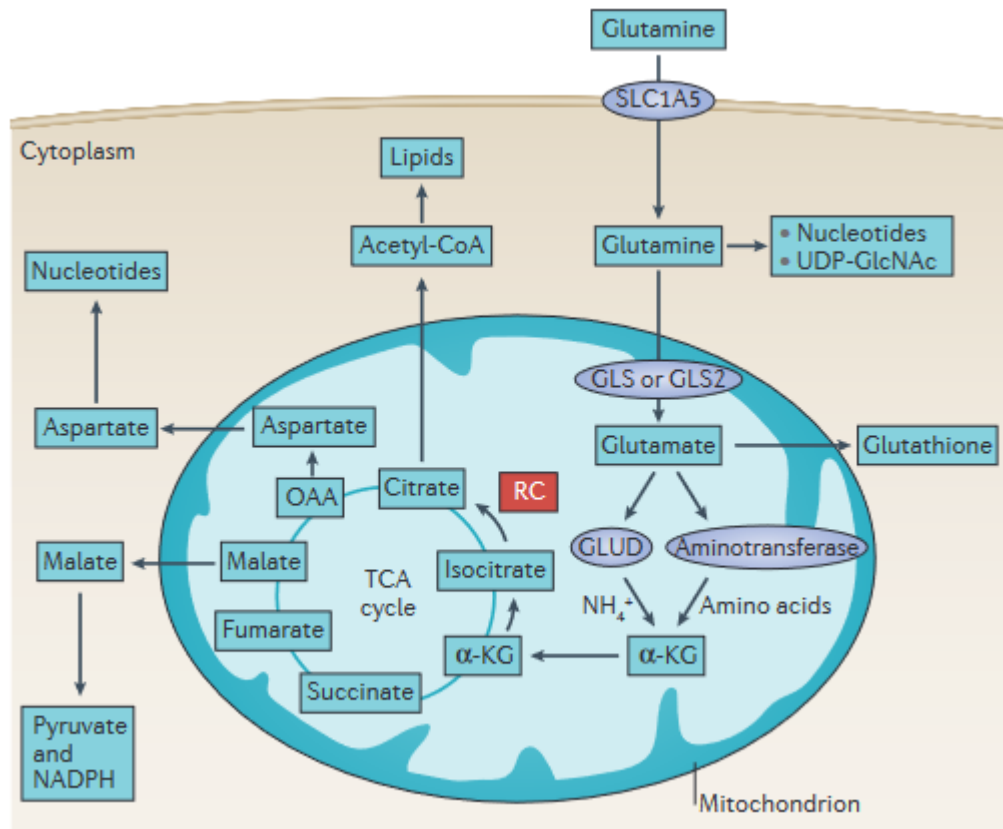


Figure 5. Metabolic and biosynthetic fates of glutamine. Figure reprinted with permission from Altman BJ, Stine ZE, and Dang CV. From *Krebs to clinic: glutamine metabolism to cancer therapy*. *Nature reviews Cancer*. 2016;16(10):619-634.³⁴

GLS has two isoforms, GLS (also called GLS1) and GLS2, however GLS2 is not widely expressed in tumors and will not be discussed here further.^{35,40} GLS has increased activity during metabolic reprogramming of cancer cells after exposure to stressors such as AVA therapy, and its expression has been correlated with a multitude of oncogenic pathways including HIF-1 α , cMYC, EGFR, RAS/MAPK, and PI3K/AKT/mTOR.^{34,41} Importantly, a high expression of GLS has been reported in many solid tumors and it is correlated with poor disease outcomes. Specifically within ovarian cancer, the median OS was almost two years shorter for patients with a high versus a low expression level of GLS (35.9 vs 58.6 months, respectively; Figure 6).³⁵ Therefore, GLS inhibitor (GLSi) therapy is a potentially valuable therapeutic strategy.

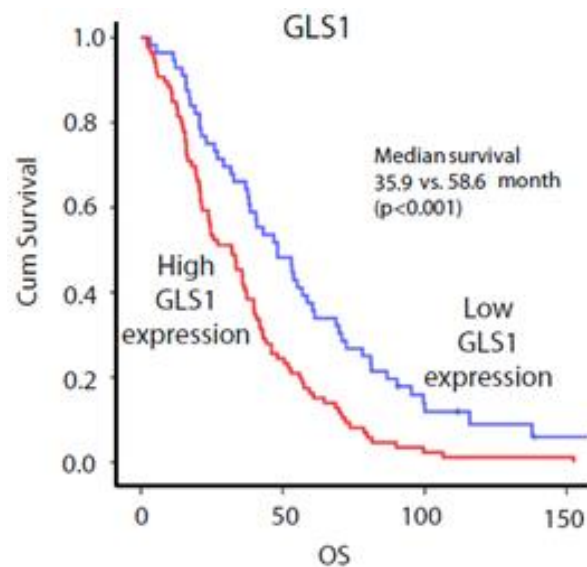


Figure 6. Kaplan-Meier curve of disease-specific survival as it relates to GLS1 expression. In a cohort of 129 patients with HGSC, median survival was 35.9 vs 58.6 months for patients with a high vs. a low GLS1 expression level, respectively ($p < 0.001$). Figure reprinted with permission from www.kmplot.com that is published with open access under the CC-BY Creative Commons attribution license; the content is free to download and adapt given appropriate attribution to the original article: Gyorffy B, Lánczky A, Szállási Z. Implementing an online tool for genome-wide validation of survival-associated biomarkers in ovarian-cancer using microarray data from 1287 patients. *Endocr Relat Cancer*. 2012;19(2):197-208.³

Glutaminase inhibitor (GLSi) targeted therapy

Several GLS inhibitors have been commercially developed, but CB-839 (Telaglenastat) is the agent most robustly investigated.⁴² CB-839 has been studied in over 10 clinical trials evaluating its efficacy in solid tumors as both single agent therapy and also in combination with traditional chemotherapeutics.⁴³⁻⁵⁵ Targeting GLS with GLSi therapy *in vitro* in ovarian cancer cell lines has demonstrated a synergistic effect with standard chemotherapy.⁵⁶ Additionally, and perhaps more importantly, GLSi has been shown to re-sensitize cell lines that are resistant to both platinum and taxane chemotherapy.⁵⁷ Despite this exciting preclinical work, the potential for GLSi in ovarian cancer has yet to be realized. While there are multiple active clinical trials investigating the use of GLSi in ovarian cancer treatment,^{44,54} the

use of a GLSi in the context of AVA-resistant ovarian cancer has not been investigated.

Given the nearly ubiquitous use of AVA treatment in ovarian cancer and the high rates of adaptive resistance that develop in response to therapy, there is an ever-expanding patient population with AVA-resistant disease that have limited treatment options available. It is therefore imperative that the relationship between glutamine metabolism and AVA-resistance be more well defined in pursuing this as a therapeutic strategy in the clinical realm. The purpose of this work is to explore the metabolic adaptations that occur in adaptive resistance to AVA therapy and to determine whether these changes could render AVA-resistant ovarian cancers susceptible to treatment with GLSi targeted therapy.

HYPOTHESIS AND SPECIFIC AIMS

Hypothesis: Hypoxia-mediated glutamine dependence in AVA-resistant ovarian cancer will make it susceptible to GLS inhibitor therapy.

Figure 7, on the next page, demonstrates a graphical representation of the conceptual framework of this hypothesis.

Specific Aim 1: To test the *in vitro* effects of hypoxia on glutamine metabolism.

Specific Aim 2: To test the *in vitro* effects of glutaminase inhibition on ovarian cancer cells and endothelial cells under hypoxic conditions.

Specific Aim 3: To test the biological relevance of glutaminase inhibition in well-characterized mouse models of adaptive resistance to AVA therapy in ovarian cancer.

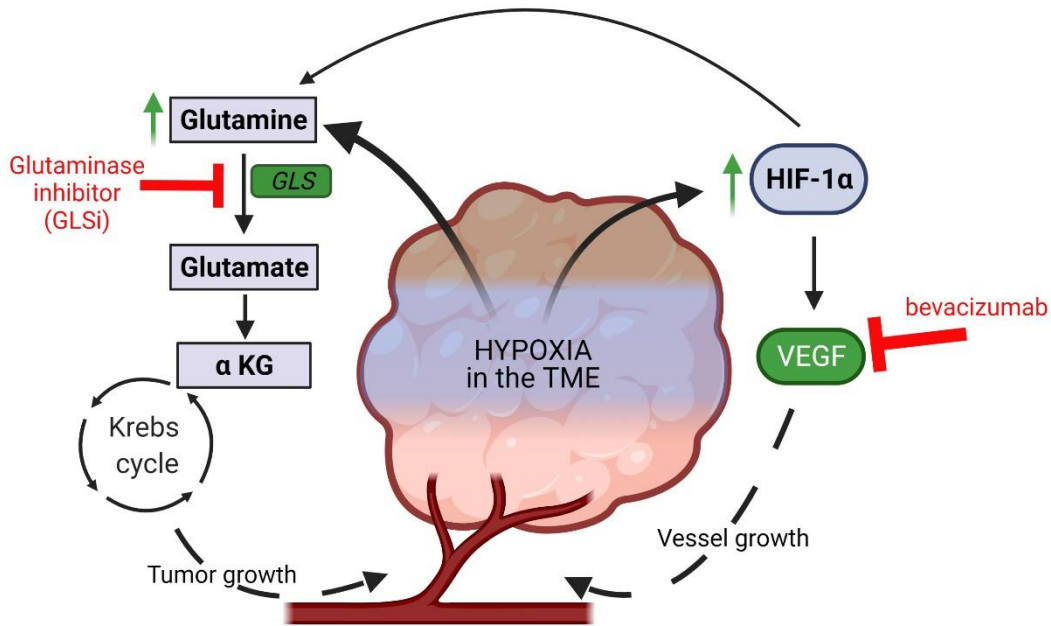


Figure 7. Working model of the central hypothesis. Exposure to bevacizumab (anti-VEGF monoclonal antibody, AVA) creates a hypoxic TME leading to an increased expression of hypoxia inducible factor 1 alpha (HIF-1 α). This hypoxic trigger then creates a metabolic shift toward dependence on glutamine catabolism for tumor growth and progression. The hypoxia-induced metabolic adaptation represents a potential vulnerability that could be exploited by inhibiting the GLS enzyme with a GLS inhibitor (GLSi) in combination with AVA treatment such as bevacizumab. Figure Created with BioRender.com. TME, tumor microenvironment; α KG, alpha ketoglutarate; HIF-1 α , hypoxia inducible factor-1 alpha.

MATERIALS AND METHODS

Cell lines and culture conditions

The human ovarian cancer cell lines SKOV3ipluc (RRID: CVCL_0C84), OVCAR5 (RRID: CVCL_1628), and OVCAR8 (RRID: CVCL_1629) were obtained from the ATCC and The University of Texas MD Anderson Cancer Center Cytogenetics and Cell Authentication Core. The immortalized human vascular endothelial cell line RF24 (RRID: CVCL_AX74) was obtained from Dr. Lee Ellis (MD Anderson Cancer Center). SKOV3ipluc and OVCAR8 cells were cultured in RPMI 1640 medium (HyClone) supplemented with 10% fetal bovine serum (Sigma-Aldrich) and 1% gentamycin. OVCAR5 cells were cultured in Dulbecco's modified Eagle's medium supplemented with 10% fetal bovine serum and 1% gentamycin. RF24 cells were cultured in minimum essential medium supplemented with 10% fetal bovine serum, sodium pyruvate, non-essential amino acids, and 1% gentamycin. All cells were cultured at 37°C with 5% CO₂ and ambient atmospheric O₂ unless performing a hypoxia experiment, in which case they were cultured with 1% O₂ as indicated. All cell lines were authenticated by the Cytogenetics and Cell Authentication Core using short tandem repeat fingerprinting and were tested for mycoplasma contamination using polymerase chain reaction. Cells were used within 20 passages after thawing for in vitro experiments and 10 passages after thawing for in vivo experiments.

Cell viability assay

To evaluate the cytotoxic effects of GLSi and bevacizumab as monotherapy and in combination on cell viability, ovarian cancer cells (SKOV3ip1, OVCAR5, and OVCAR8) were seeded in a 96-well plate at a density of 3,000 cells per well in 100- μ L total volume in quadruplicates. Cells were incubated for 24 hours, and after

demonstration of adequate attachment, the culture medium was removed and replaced with a medium containing serial dilutions of GLSi and bevacizumab. The cells were then incubated for 24, 48, or 72 hours depending on the experimental oxygen conditions. Following incubation, the cells were treated with a 0.05% MTT solution for 2-4 hours. The supernatant was then gently removed, and the MTT formazan was dissolved in 100 μ L of dimethyl sulfoxide. The absorbance was subsequently read at 570 nm using a BioTek uQuant microplate spectrophotometer. All experiments were performed in triplicate. Dose-response curves were plotted using Prism software (version 8.0.0; GraphPad Software).

Western blotting

Extraction of total protein cell lysates was performed using modified RIPA buffer with protease and phosphatase inhibitors. BCA Protein Assay Reagent (Thermo Fisher Scientific) was then used to measure protein concentrations. Protein expression for each lysate was subsequently detected via Western blotting of a sodium dodecyl sulfate-polyacrylamide gel electrophoresis separation gel using a primary antibody against GLS (cat. #12855-1-AP; Proteintech). The antibody was incubated overnight at 4°C and then incubated with corresponding horseradish peroxidase-linked whole secondary antibodies. A chemiluminescence assay using a Western Lightning PLUS ECL Kit (PerkinElmer) was performed to expose the membranes and protein bands were quantified using densitometry with ImageJ software (National Institutes of Health). β -actin was used as a sample loading control for all reads.

Quantitative RT-PCR (qRT-PCR)

Relative levels of mRNA expression of GLS were detected using the qRT-PCR method as described before.³⁸ Briefly, each qRT-PCR was carried out with 1 µg of RNA isolated from cells using RNeasy Mini Kits (Qiagen, CA) and reverse transcribed using High-Capacity cDNA Reverse Transcription Kit (Applied Biosystems Inc.) according to the manufacturer's protocol. The cDNA synthesized was then used as a template in the qRT-PCR using the specific GLS TaqMan Gene expression probes (Hs0104020_m1, ThermoFisher). Quantitative RT-PCR was performed on a 7500 Real-Time PCR System (Applied Biosystems, Inc.). The 18s rRNA was used as endogenous control, and relative mRNA expression was calculated using $2^{-\Delta\Delta CT}$ method.⁵⁸

GLS gene silencing by small interfering RNA

Small interfering RNA (siRNA) targeted to GLS was purchased from Sigma-Aldrich. In vitro transient transfection was performed as described previously.⁵⁹ Briefly, the cells were transfected with a GLS1-specific or scrambled (control) siRNA using lipofectamine 2000 reagent (Invitrogen, Carlsbad, CA). siRNA with a nonspecific function that shared no sequence homology with any known mRNA in a BLAST search was used to control the target siRNA (Mission siRNA Universal Negative Control#1, Sigma). At selected time intervals, cells were harvested to measure mRNA levels of *GLS1* using qRT-PCR.

In vivo models of ovarian cancer

All animal protocols were approved by the MD Anderson Institutional Animal Care and Use Committee. All animal experiments were performed with 6- to 8-week-

old female athymic nude mice (NCr-nude) obtained from Taconic Biosciences. The mice were housed five per cage under pathogen-free conditions at a constant temperature and humidity. All mice were fed a regular diet and water *ad libitum* according to the guidelines of the American Association for Laboratory Animal Science and the U.S. Public Health Service Policy on Humane Care and Use of Laboratory Animals. Investigators sacrificed the mice via carbon dioxide euthanasia followed by cervical dislocation once the mice were moribund.

To establish xenograft models for all mouse experiments, luciferase-labeled SKOV3ip1 ovarian cancer cells were cultured to 70-90% confluence and then trypsinized, washed twice with phosphate-buffered saline, and resuspended in ice-cold Hank's Balanced Salt Solution (cat. #21-021-CV; Cellgro). The mice were then inoculated with 1×10^6 SKOV3ip1 cells via intraperitoneal injection to the right side of the abdomen. Tumor establishment was subsequently confirmed after injection of 200 μ L of 14.3 mg/mL luciferin (cat. #LUCK-1G; GoldBio) using a Xenogen IVIS *in vivo* imaging system. Mice without tumor uptake were removed from the experiment. Following confirmation of disease burden, all mice in the therapeutic experiment were randomly assigned to the following treatment groups: vehicle control, bevacizumab (AVA; 6.25 mg/kg, intraperitoneally, twice a week), GLSi (IACS-012031, 200 mg/kg given orally twice daily, five days a week), or a combination of the two at these doses (n = 15 for all groups).

In the AVA-resistance model, twice-weekly treatment with bevacizumab (AVA) was initiated upon confirmation of tumor uptake. Tumor burden was subsequently assessed weekly via IVIS imaging (Xenogen), and the mice were placed in two groups: AVA-sensitive and AVA-resistant. Sensitivity to AVA therapy

was defined as a decrease or plateau in the relative intensity of bioluminescent signaling over three weeks of treatment. The AVA-sensitive mice were sacrificed approximately one week later to confirm that they truly had sensitive phenotypes. Resistance to AVA therapy was defined as an initial decrease then steady increase in the relative intensity of bioluminescent signaling. The resistant group was then separated into two groups: control (AVA plus vehicle control given via oral gavage twice a day, n = 20) and AVA treatment (AVA plus GLSi given via oral gavage twice a day, n = 25). The treatment in both groups continued until each mouse became moribund at which point, they were sacrificed. The mice were monitored daily for adverse effects of treatment, and their body weights were measured weekly. Survival time was calculated for each mouse as the number of days from the date of inoculation of SKOV3ip1 cells to the date of euthanasia.

Mouse tumor weights, nodule numbers, distribution of metastasis, and presence of ascites were recorded at the time of gross necropsy. All tumor tissues were dissected, and samples were snap-frozen for later protein or RNA analysis (e.g., DESI-MS, LC-MS), fixed in formalin for paraffin embedding, or snap-frozen in optimal cutting temperature compound (Mercedes Scientific) for frozen slide preparation.

Bevacizumab was obtained from MD Anderson pharmacy. The glutaminase inhibitor, IACS-012031, was obtained from the MD Anderson Institute for Applied Cancer Science and reconstituted in 25% aqueous 2-hydroxypropyl- β -cyclodextrin (cat. #H107-100G; Sigma-Aldrich) in phosphate-buffered saline at a dose of 25 mg/mL. This was administered via oral gavage as above.

IHC staining

All tumor samples subjected to IHC staining were collected from the *in vivo* experiment. Formalin-fixed, paraffin-embedded tumor sections were used for staining for anti-Ki67 (1:100, cat #RB-9043-PI; NeoMarkers). Paraffin slides were prepared via deparaffinization and antigen retrieval, whereas frozen slides were prepared via cold acetone fixation. This was followed by endogenous peroxide blocking with 3% hydrogen peroxide and a protein block with 4% fish gelatin. All samples were incubated with a primary antibody diluted in 4% fish gelatin overnight and then incubated with either a peroxidase-conjugated goat anti-rabbit or anti-mouse secondary antibody for one hour at room temperature.

Frozen slides were used for staining for CD31 (1:800, cat. #53370; BD Pharmingen) and CA9 (1:100, cat# NB100-417SS; Novus Biologicals) using goat anti-rat and goat anti-rabbit horseradish peroxidase-linked secondary antibodies, respectively (1:250, cat. #112-035-167; Jackson ImmunoResearch). Frozen slides were prepared by first fixing slides in cold acetone for 10 minutes and then washing them in phosphate-buffered saline and blocking with endogenous peroxidase and 3% H₂O₂ in methanol. All samples were incubated with a primary antibody diluted in protein block (5% normal horse serum and 1% normal goat serum in phosphate-buffered saline) overnight at 4°C. The slides were incubated with a secondary antibody for one hour and subsequently incubated with DAB (Invitrogen, Cat. #750118). Microscopic assessment of DAB staining was performed for all slides to monitor appropriate staining density. The slides were counterstained with hematoxylin (Gill 3). Quantification of IHC staining was performed by randomly selecting five fields at 200x magnification per slide and manually counting stained

nuclei in each field. Mean cell count and standard deviation (SD) was calculated, and treatment groups were compared using the Student t-test.

Polar metabolite extraction from tissue

The protocol was modified from Zhou et al, 2020.⁶⁰ To minimize metabolite degradation, tumor tissue samples were kept on dry ice throughout the LC-MS experiment. Briefly, 30-66 mg of each tissue sample was quickly weighed in a homogenizer tube previously filled with beads. A prechilled methanol/water (1:1, v/v) solution was added to the tube based on the weight of the measured tissue (5 mL per 1 g of tissue, or 125 μ L per 25 mg of tissue). The samples were then homogenized using a Precellys homogenizer (Bertin Instruments) at 4°C and 6,500 rpm using two cycles of 25 seconds with 30-second intervals. Afterward, 100 μ L of the tissue homogenate was transferred to a fresh tube, and 500 μ L of methanol/water (1:1, v/v) solution and 500 μ L of chloroform were added to the samples and they were vortexed for two minutes at 4°C and centrifuged at 16,000g for 10 minutes at 4°C. A total of 500 μ L of polar metabolite extract was then dried in a vacuum evaporator. The dried metabolites were reconstituted in 200 μ L of methanol/water (1:1, v/v) solution, sonicated for 10 minutes, and filtered through an Agilent 0.2- μ m Econofilter. The filtrate was then transferred into LC vials for analysis.

LC-MS protocol and data analysis

A 10 μ L tumor sample prepared in the manner outlined above was injected for analysis into an Agilent 6520 Q-TOF LC/MS machine with an ACQUITY UPLC BEH C18 Column (130 Å, 1.7 μ m, 2.1 mm x 150 mm) coupled with VanGuard Pre-Columns and an XBridge BEH Amide XP Column (130 Å, 2.5 μ m, 4.6 mm x 150

mm) coupled with an XBridge BEH Amide XP VanGuard Cartridge (130 Å, 2.5 µm, 2.1 mm x 5 mm). The column compartment was set at 40°C, and the analysis was performed in both positive and negative modes. One hundred microliters of sample filtrate was transferred to LC vials, and 10 µL of each filtered sample was pooled to form the quality control samples. For analysis of the C18 column, mobile phase A consisted of water with 0.1% formic acid, whereas mobile phase B contained acetonitrile in 0.1% formic acid. The gradient method using the C18 column was as follows: 0 minutes: 1% B; 1 minute: 1% B; 8 minutes: 99% B; 13 minutes: 85% B; 13.1 minutes: 1% B; 16 minutes: 1% B. For analysis with the HILIC column, the mobile phase A was 10 mM ammonium formate in water with 0.1% formic acid, whereas mobile phase B contained 10 mM ammonium formate in acetonitrile with 0.1% formic acid. The gradient method using the HILIC column was as follows: 0 minutes: 99% B; 11.8 minutes: 20% B; 12.5 minutes: 99% B; 14.7 minutes: 99% B. The metabolite peaks were extracted for the analysis using Agilent MassHunter Profinder software based on our in-house library of metabolites. Any metabolites whose relative SD was greater than 30% in the QC measurements were excluded from further analysis. The metabolite peak areas in the spectrum were normalized according to the weight of the tissue. Other downstream analyses were performed using MetaboAnalyst software version 5.0 and data were then presented with the aid of Graphpad prism version 8.0.0.

DESI-MS Imaging and SAM Analysis

Tumor tissues were flash-frozen and stored at -80°C prior to analysis. Frozen tissues were sectioned at 12 µm thickness, thaw-mounted onto glass slides, and immediately analyzed using a Q Exactive Focus or Q Exactive HF Orbitrap mass

spectrometer (Thermo Fisher Scientific) coupled to a 2D OmniSpray stage (Prosolia Inc.) and a laboratory-built DESI sprayer. DESI-MS imaging was performed in the negative ion mode at a spatial resolution of 200 μm using a mass resolving power of 70,000 (m/z 200) and an instrument method optimized for enhanced detection of small metabolite species from m/z 80-500. A histologically compatible solvent system comprised of methanol:acetone 4:1 (v/v) was used as the DESI spray solvent, at a flow rate of 5.0 $\mu\text{L}/\text{min}$. DESI-MS ion images were assembled and visualized using Firefly (Prosolia, Inc.) and BioMap (Novartis) software. Ions of interest were tentatively identified using high mass accuracy measurements and tandem mass spectrometry experiments.

After DESI-MS imaging, the analyzed tissue sections were stained with hematoxylin and eosin and regions of tumor, stroma, and necrosis were annotated by D.G. within each sample. Mass spectra were extracted from pixels corresponding to tumor regions within the DESI-MS dataset using MSiReader software. The resulting ion intensity matrix was processed by binning each m/z value to the nearest thousandth and removing peaks that were present in less than 20% of the extracted pixels. The extracted DESI-MS data was analyzed using significance analysis of microarrays (SAM), a modified significance test to identify statistically significant alterations in relative abundance for specific mass-to-charge (m/z) values.⁶¹ Multiclass SAM was performed in R using the “samr” package to identify features with significantly altered abundance among treatment groups. A false discovery rate (FDR) of 5% was applied to identify m/z values with significant differences in relative abundance among treatment groups. Ion intensities for selected metabolites of

interest were plotted in GraphPad Prism (version 9.3.0) and subjected to one-way ANOVA with Tukey's post-hoc test for pairwise comparisons.

Hyperpolarized ^{13}C -pyruvate sample preparation

A solution of 20 μL of ^{13}C pyruvic acid (ISOTECH; Sigma-Aldrich), 15 mM OX63 trityl radical (GE Healthcare), and 1.5 mM gadolinium chelate (ProHance) was polarized at 3.35 T and 1.4 K using dynamic nuclear polarization (HyperSense; Oxford Instruments) for one hour. A frozen ^{13}C -pyruvate sample was rapidly dissolved in 4 mL of superheated alkaline buffer containing 100 mg/L EDTA, 40 mM NaOH, 40 mM TRIS buffer, and 30 mM NaCl. The final concentration of pyruvate to be injected into the mouse tail vein was 80 mM, with a physiologic pH of about 7.4. In total, 200 μL of hyperpolarized pyruvate was injected into mice using a tail vein catheter for 8-10 seconds.

Animal handling during magnetic resonance imaging experiments

For magnetic resonance imaging (MRI) experiments, a 7T Bruker BioSpin MRI scanner (horizontal bore) was used. Mice were anesthetized using isoflurane in an anesthesia chamber with scavenging. The animals were fixed in a holder specially designed for mice and placed in the MRI coil equipped with a nose cone for inhaled analgesia. A respiration monitoring pad and body temperature-maintaining heated pad were used during the MRI experiments.

T2-weighted proton MRI

Conventional anatomic magnetic resonance images of mice were acquired using multislice T2-weighted rapid acquisition with a relaxation enhancement sequence. Images with different views, including axial, coronal, and sagittal views,

were acquired to identify tumors and regions of interest in the flanks of the mice. The imaging parameters for the T2-weighted scans were an echo time of 15 milliseconds, repetition time of 2.5 seconds, 4-cm field of view, 256 μm \times 256 μm in-plane resolution, 10 slices with thicknesses of one mm, and four image averages.

In vivo ^{13}C magnetic resonance spectroscopy

A series of slab-selective ^{13}C spectra with a slab thickness of 8 mm were acquired right after injection of mice with hyperpolarized pyruvate using an SP Flash sequence. The intraperitoneal tumor locations and similar sizes of the tumors in the experimental mice used in this study increased the precision of slab placement through most of the ovarian tumors and limited the contribution of nonmalignant signals consistently throughout the experiments. A total of 90 transients were acquired using a delay time between each transient of two seconds (total time, three minutes). For each transient, a 15° flip angle excitation Gaussian pulse and 2,048 data points were used. A small 8M ^{13}C urea phantom injected with gadolinium-DPTA was used in each mouse experiment for chemical shift referencing. Experimental data were processed on the MATLAB programming language (The MathWorks, Inc.) and TopSpin (Bruker BioSpin) platforms. Phase correction and 10- to 15-Hz line broadening were introduced to each individual spectrum. The areas under the spectral peaks within the frequency range for pyruvate and lactate were integrated over the entire array. The lactate-to-pyruvate metabolic flux ratios (lactate/pyruvate) were estimated by calculating the individual integration of lactate and pyruvate spectral signals between treatment groups and comparing the change in signal over time.

Statistical analysis

Differences between groups were evaluated using the Student t-test or Mann-Whitney U test according to data distribution and variance homogeneity. One-way differences between two groups were evaluated using the Student t-test or Mann-Whitney U test according to data distribution and variance homogeneity, whereas one-way analysis of variance was used for multiple group comparison. For survival experiments, Kaplan-Meier analysis and a log-rank test were performed to explain differences in survival. All statistical analyses were conducted using Prism software (version 8.0.0). The p values were two-tailed and values less than 0.05 were considered significant. All results were presented as means (\pm SEM or SD).

RESULTS

Treatment with, and adaptive resistance to, AVA therapy induces alterations in glutamine metabolism in vitro

Given the known inherent hypoxia in the TME and the added hypoxic stress imposed by AVA therapy,^{19,20} we set out to understand the impact of hypoxia extremes on glutamine metabolism. To do so, we first evaluated the *in vitro* GLS expression in the ovarian cancer cell line OVCAR8 and endothelial cancer cell line RF24 when cultured in hypoxic conditions at 1% O₂ versus normal atmospheric oxygen (i.e. 20% O₂). We did this in concert with measuring the HIF-1 α expression level. Our results indicate that GLS and HIF-1 α expression in both cell lines was higher under hypoxic rather than under normoxic conditions (Figure 8 A, B).

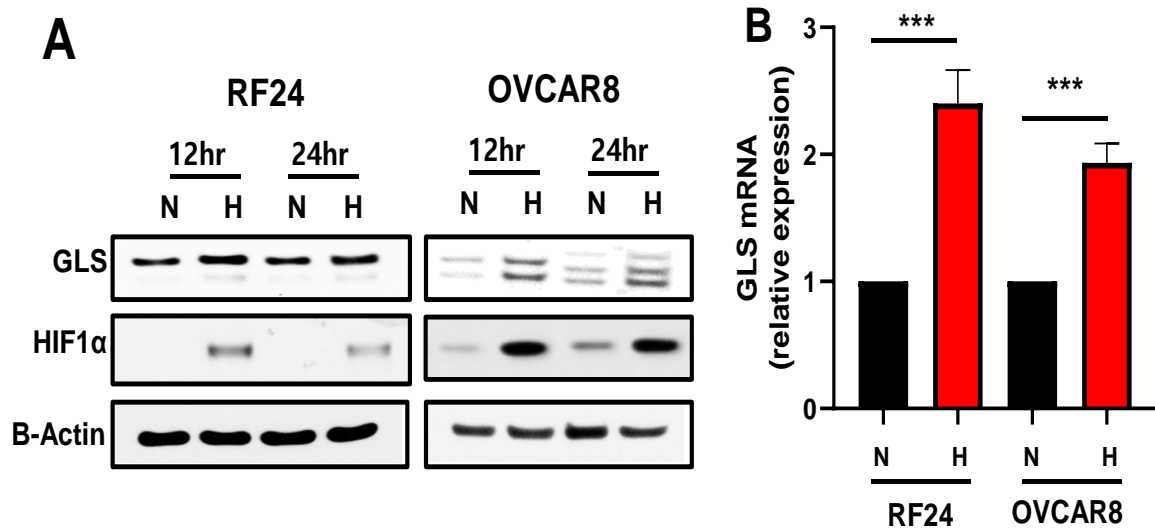


Figure 8. Metabolic alterations in hypoxia and resulting from AVA therapy. RF24 and OVCAR8 cells were cultured in normoxia (N) or hypoxia (H) for 12 and 24 hours. GLS and HIF-1 α protein (A) and GLS mRNA (B) expression levels in both cell lines were measured. Error bars indicate standard deviation (SD), *** $p < 0.001$.

To evaluate the downstream metabolic effects of an increased GLS expression in hypoxia, we performed an *in vivo* investigation using an orthotopic SKOV3ip1 model of ovarian cancer with adaptive resistance to AVA therapy with bevacizumab (Figure 9). In this experiment, 60 nude mice inoculated with luciferase labeled cells received either a vehicle control (200 μ L) or AVA therapy (200 μ L, 6.25 mg/kg) via intraperitoneal (i.p) injection twice weekly until resistance to AVA therapy emerged. The resistance rate was 87% (n = 52).

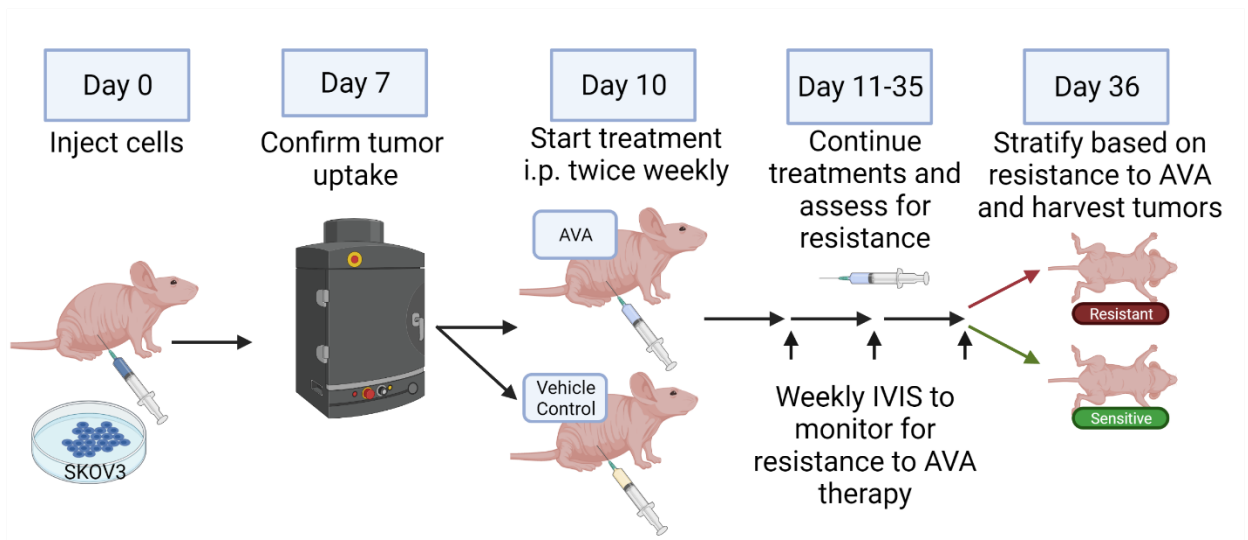


Figure 9. *In vivo* model of adaptive resistance to AVA therapy. Female nude mice were inoculated with 1×10^6 luciferase labeled SKOV3ip1 ovarian cancer cells. After confirming tumor uptake, mice were randomized to receive either a vehicle control or AVA therapy with bevacizumab (6.25 mg/kg). Serial imaging was performed on control mice to assess tumor growth and on AVA-treated mice to monitor for resistance to therapy. Tumors were harvested once resistance was observed.

All mice underwent weekly bioluminescence imaging with radiance scores tracked over time for the AVA-treated mice in order to stratify them based on sensitivity or resistance to AVA therapy as outlined in the Materials and Methods (Figure 10).

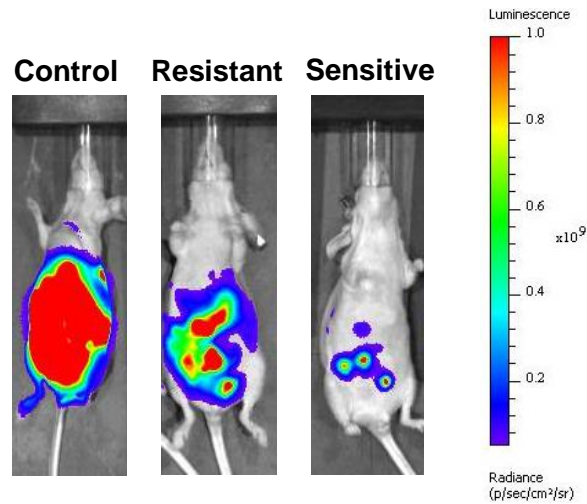


Figure 10. Adaptive resistance to AVA therapy. Images of nude mice obtained via an *in vivo* imaging system (IVIS) approximately six weeks after inoculation with 1×10^6 SKOV3ip1 cells. Mice received either a vehicle control or bevacizumab (6.25 mg/kg twice weekly) and were imaged weekly until resistance emerged.

Tumors were harvested after the mice demonstrated resistance to AVA treatment and markers of hypoxic stress using immunohistochemical (IHC) staining were assessed. Compared with control tumors, all AVA-treated tumors had higher levels of the hypoxia marker CA9 ($p < 0.01$, Figure 11A, B). As anticipated, the AVA-sensitive tumors demonstrated a reduced vascular density with lower levels of the endothelial cell marker CD31 compared with control tumors or with those that were resistant to AVA treatment ($p < 0.001$, Figure 11 C, D).

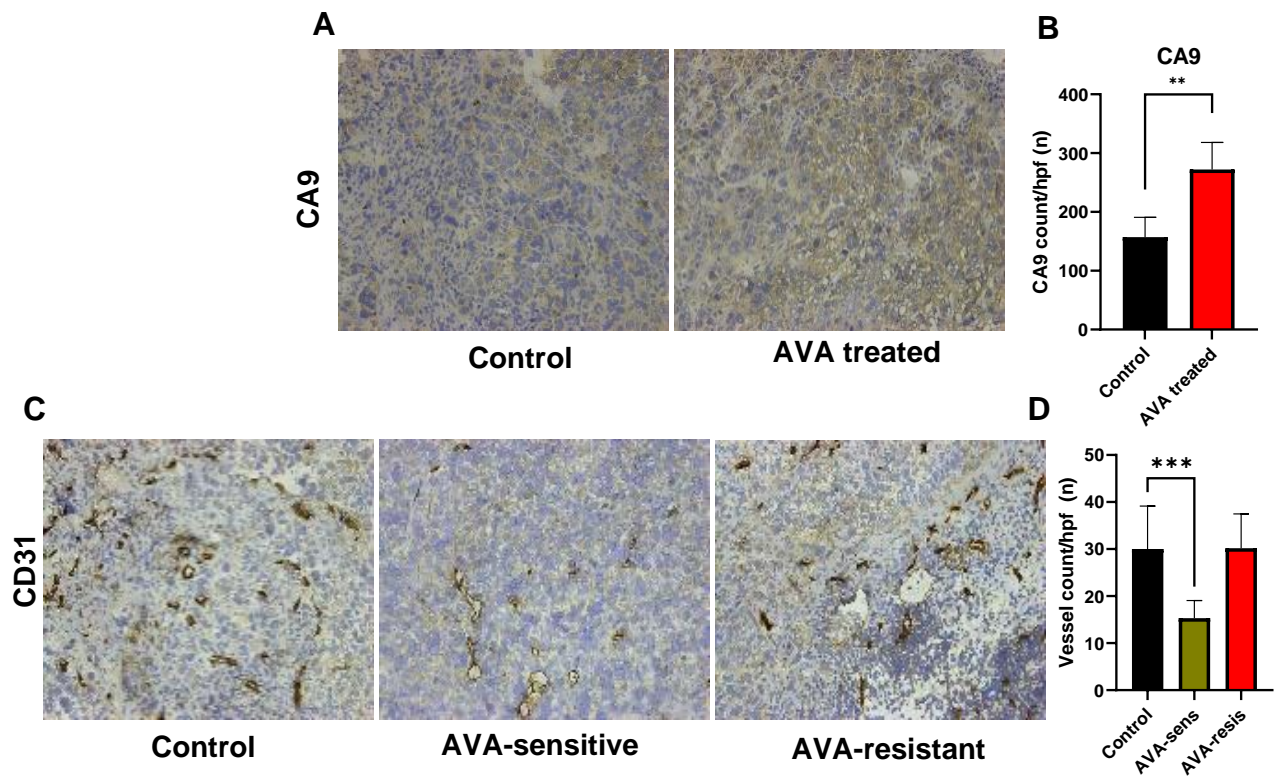


Figure 11. Effect of AVA resistance on markers of hypoxia and vascular cell density. (A) IHC staining of frozen mouse ovarian tumors for the hypoxia marker CA9 in control vs. AVA treated (bevacizumab 6.25 mg/kg i.p. twice weekly) tumors. (B) Quantification of CA9 staining in control vs. AVA treated tumors per high power field, error bars indicate standard deviation (SD), ** $p < 0.01$. (C) IHC staining of frozen mouse ovarian tumors for the endothelial cell marker CD31 in control vs. AVA-sensitive or AVA-resistant tumors. (D) Quantification of vessel densities in control, AVA-sensitive, and AVA-resistant tumor samples. Error bars indicate SD. *** $p < 0.001$ compared with the control group (Student t-test). Hpf, high power field; AVA, anti-VEGF antibody (bevacizumab); AVA-sens, AVA-sensitive; AVA-resis, AVA-resistant.

After confirmation of the hypoxic stress in this orthotopic model of adaptive resistance to AVA therapy, we set out to define the specific alterations in tumor metabolism that occur in response to this stress. We first performed a quantitative metabolic analysis of the AVA-treated tumor tissues from the above *in vivo* experiment using liquid chromatography-mass spectrometry (LC-MS). These analyses revealed greater alterations in the purine synthesis pathway in AVA-resistant samples than in AVA-sensitive and vehicle-treated control samples (Figure 12, FDR < 0.05). Specifically, the results indicated a greater abundance of metabolites such as urate, xanthine, xanthosine, and 3-ureidopropionate in the AVA-resistant group than in the control group (Figure 13 $p < 0.05$ and Figure 14, FDR < 0.05).

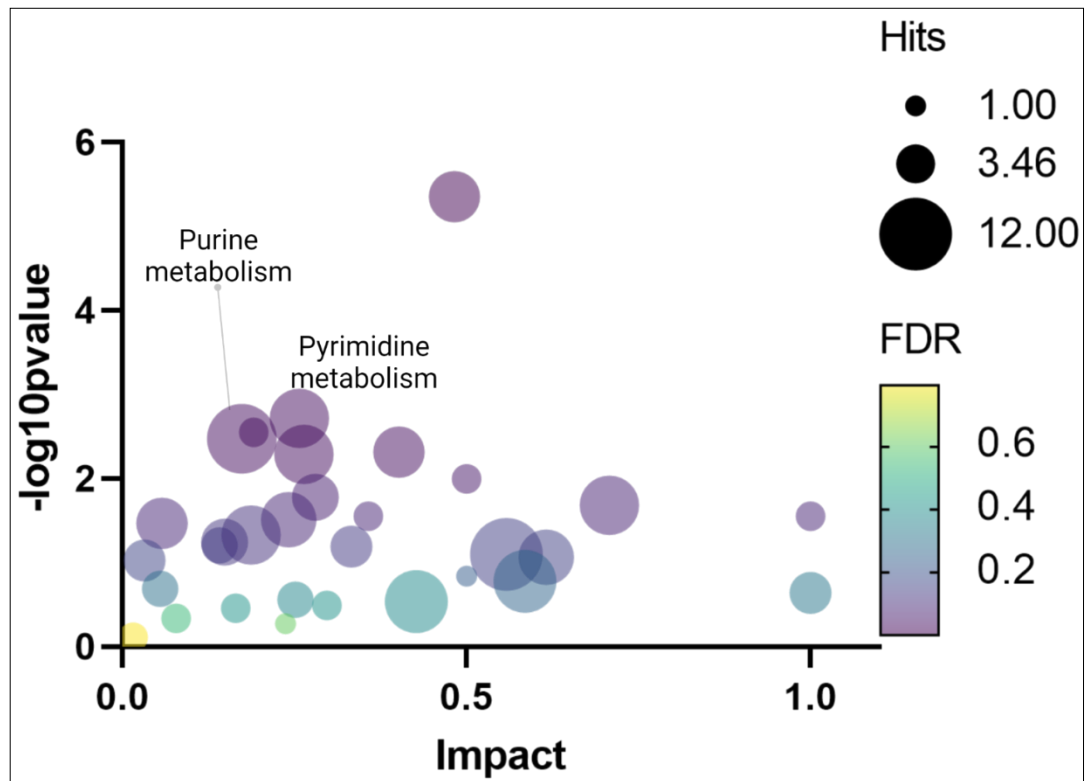


Figure 12. Impact plot of adaptive resistance to AVA therapy in an orthotopic murine model of ovarian cancer suggests alterations in purine metabolism. Plot of metabolic pathway impact analysis results upon LC-MS of control and AVA-resistant ovarian tumors from an orthotopic mouse model with SKOV3ip1 cells showing that the purine and pyrimidine metabolism in the groups differed markedly ($FDR < 0.05$). Data were generated using a MetaboAnalyst plot made with Prism software.

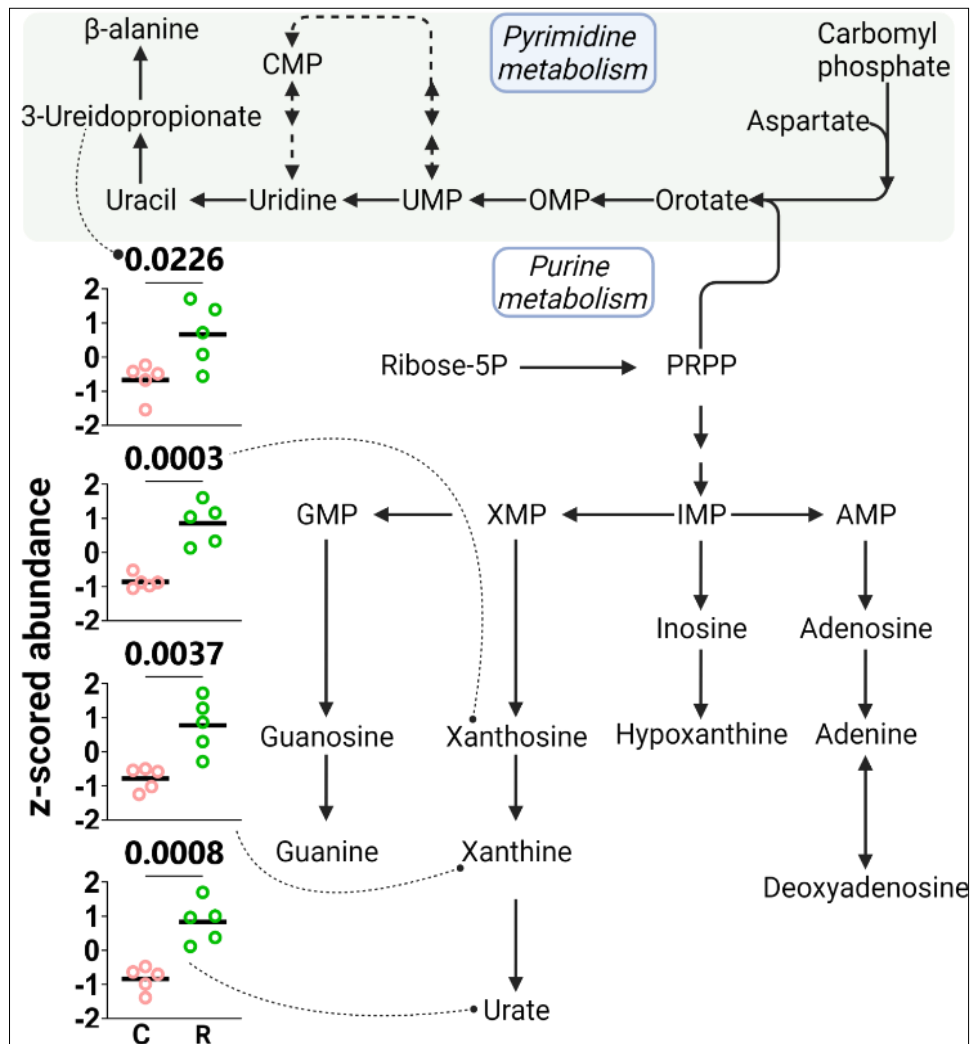


Figure 13. Metabolic alterations in the purine metabolism pathway after adaptive resistance to AVA therapy in an orthotopic murine model of ovarian cancer. Simplified diagram of the purine and pyrimidine metabolic pathways showing the key metabolites involved in nucleotide metabolism. The inserted scatter plots show significantly higher levels of downstream metabolites (urate, xanthine, xanthosine, and 3-ureidopropionate) in the AVA-resistant group than in the control group ($p < 0.05$). UMP, uridine monophosphate; OMP, orotidine 5'-monophosphate; CMP, cytidine monophosphate; PRPP, phosphoribosyl pyrophosphate; GMP,

guanosine monophosphate; XMP, xanthosine monophosphate; IMP, inosine monophosphate; AMP, adenosine monophosphate.

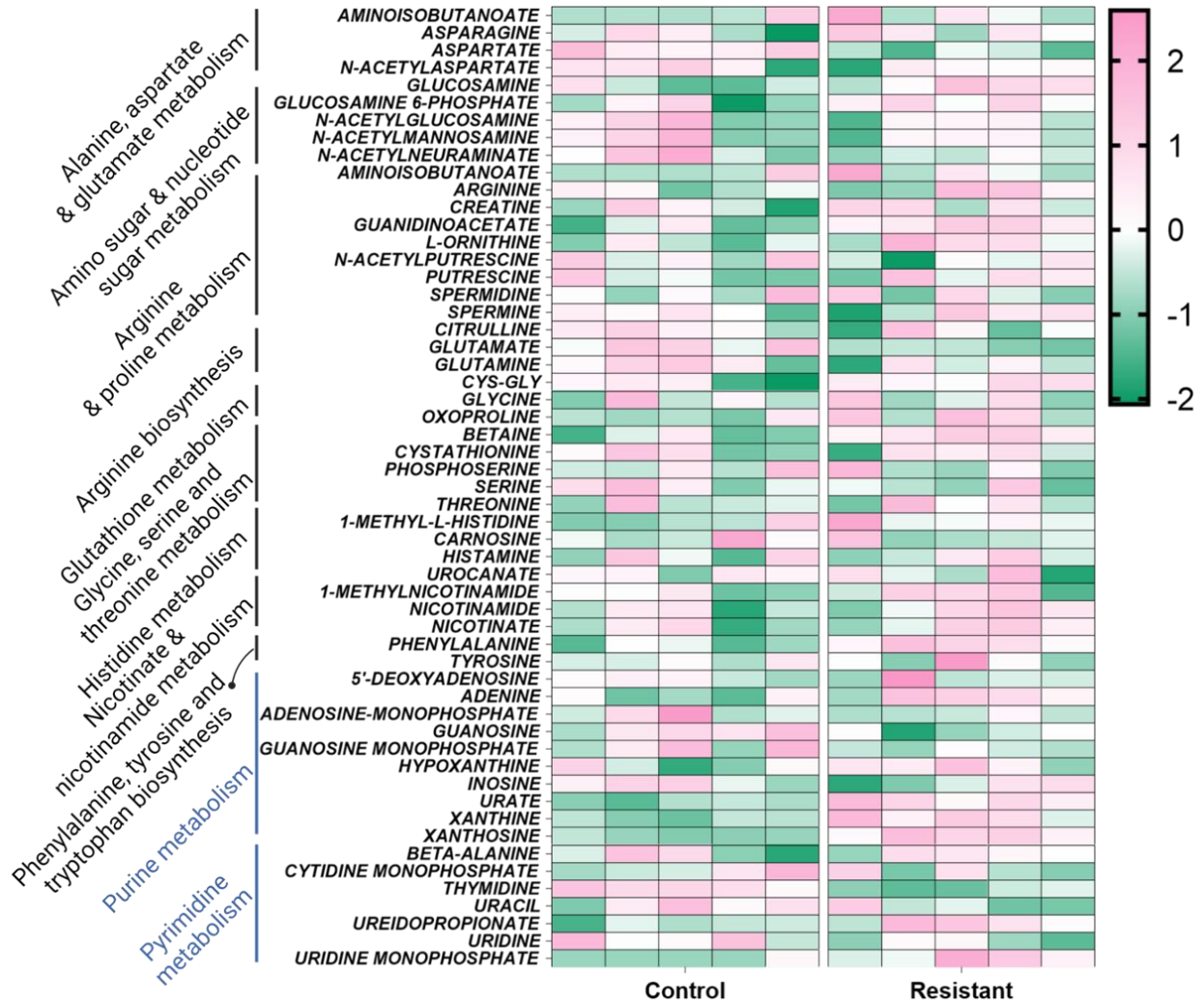


Figure 14. Heat map of altered metabolic pathways in murine ovarian cancer model with adaptive resistance to AVA therapy.

Heat map of altered metabolic pathways in control vs AVA-resistant tumor tissues from the *in vivo* experiment outlined in Figure 9. Purine and pyrimidine metabolism highlighted in blue on y axis. FDR < 0.05 with scale bar indicating log fold change $|-2 \text{ to } +2|$.

To further investigate the treatment-specific metabolic changes within the heterogeneous TME of this model, desorption electrospray ionization-mass spectrometry (DESI-MS) imaging^{62,63} of the same tumor samples was subsequently performed. Spatially resolved molecular information was selectively extracted from the DESI-MS data obtained from tumor regions within each sample, excluding adjacent stroma or necrotic tissue. Significance analysis microarray (SAM) identified alterations in the relative abundance of a variety of molecular species when comparing control to AVA-treated tumors, including multiple key intermediates in amino acid metabolism, glycolysis, and purine synthesis (Figure 15, FDR < 0.05). Higher relative abundances of xanthine and hypoxanthine were detected in the AVA-resistant tumor tissue regions relative to control, in agreement with LC-MS experiments ($p < 0.01$ and $p < 0.03$, respectively).

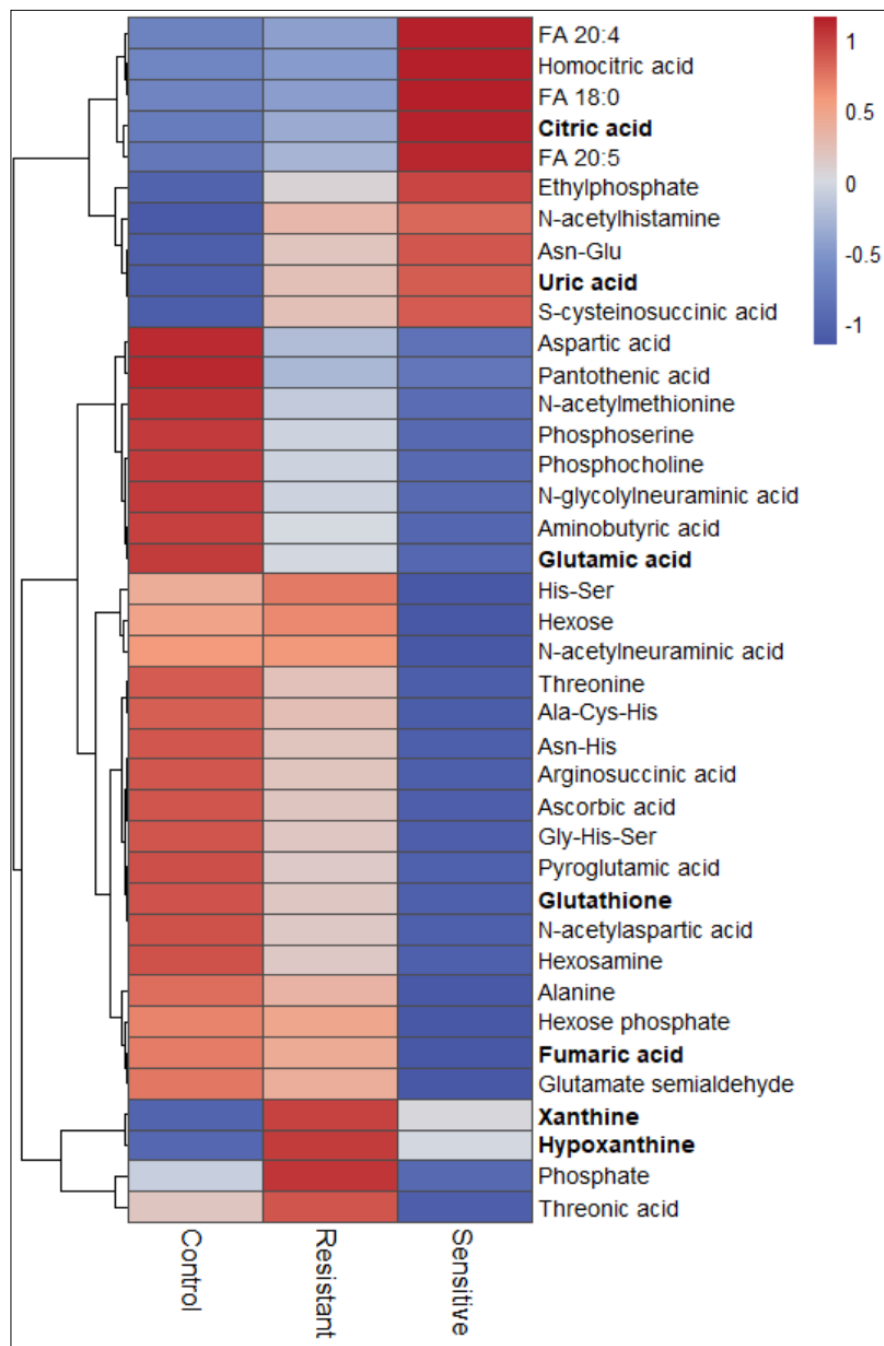


Figure 15. Heat map of metabolic alterations assessed by DESI-MS in ovarian cancer with adaptive resistance to AVA therapy. Intensity heat map for metabolites selected by SAM as significantly altered among control, AVA-resistant, and AVA-sensitive tissues (FDR < 5%) identified by DESI-MS imaging. Features were clustered using a Euclidean-distance formula according to the average signal intensity of the corresponding m/z value measured from tumor-specific regions. The color scale reflects z-score standard deviations from the mean relative abundance measured for each ion. For fatty acid (FA) species, X:Y indicates the number of carbons and double bonds, respectively.

Additionally, significant alterations in glutaminolysis metabolites were identified with increased relative abundances of glutamate relative to glutamine in AVA-resistant compared to AVA-sensitive tissues, but not when compared to control (normalized ion abundance: 7.4 vs. 5.3 and 9.1, respectively; Figures 16 and 17, $p < 0.05$). That is, the conversion of glutamine to glutamate in the AVA-resistant tumors resembled that of the control whereas there was a reduced catabolism of glutamine in the AVA-sensitive tumors. Similar trends were observed for fumarate and glutathione, both of which are downstream metabolites of glutamate (data not shown). Overall, our comprehensive mass spectral analyses of AVA-treated tumors indicate a significant role of glutamine metabolism in these tumors, particularly in AVA-resistance.

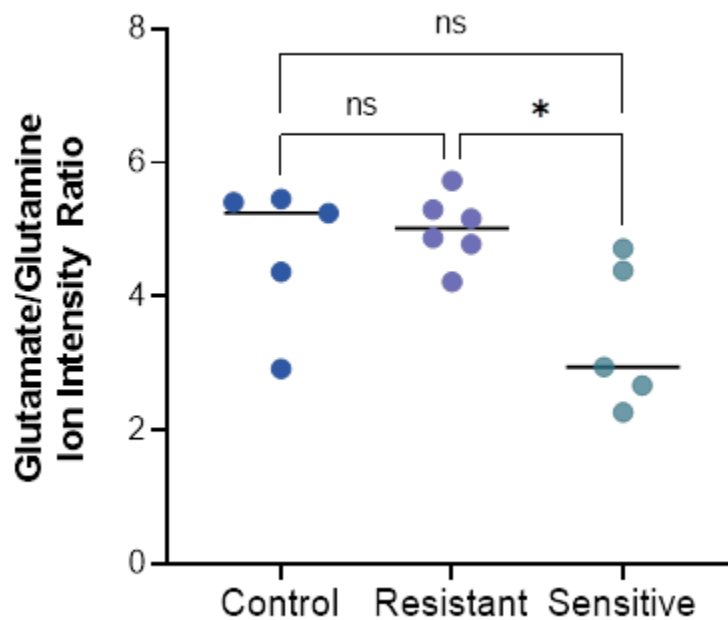


Figure 16. Normalized ion abundance ratio of glutamate to glutamine in AVA-resistance. Ion intensity ratio of glutamate to glutamine within tumor tissues from an SKOV3ip1 ovarian cancer mouse model receiving no treatment (control) vs. AVA-resistant (Resistant) or AVA-sensitive (Sensitive) tumors, as monitored by *in vitro* imaging analysis. Statistical significance was determined by Tukey's HSD post hoc test, * $p < 0.05$.

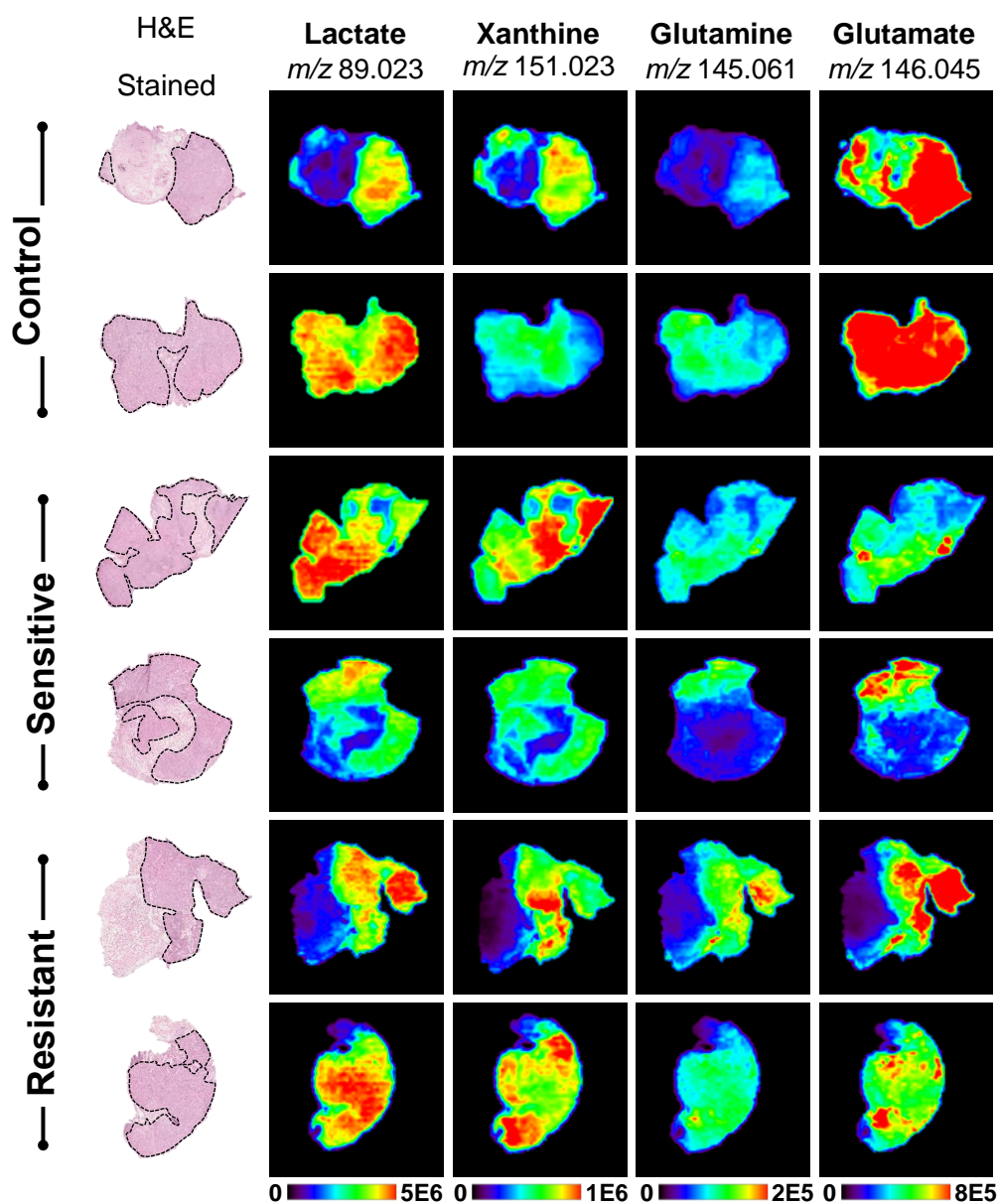


Figure 17. DESI-MS ion images of ovarian tumors with adaptive resistance to AVA therapy. DESI-MS demonstrates an increase in glutaminolysis in AVA-resistant tumors compared to control tumors, with an increased abundance of glutamate in all AVA-resistant tumors compared to AVA-sensitive tumors but not compared to control tumors. Normalized ion abundance: 7.4 vs. 5.3 and 9.1 for Resistant, Sensitive and Control, respectively, $p < 0.05$. NL, normalization level.

Hypoxia induces GLS expression in a hypoxia-inducible factor-1 α dependent manner

In order to better understand the mechanisms by which GLS expression is altered after exposure to AVA therapy, we evaluated the relationship of HIF-1 α and GLS expression. In many cancers, GLS expression has been documented to be correlated with HIF-1 α expression and level.^{20,64,65} To determine whether this is a direct correlation, we analyzed ovarian cancer cells (OVCAR8) and endothelial cells (RF24) that were transiently transfected with small interfering RNA (siRNA) targeting HIF-1 α or HIF-2 α (Figure 18). We observed that the increased GLS expression seen under hypoxic conditions (1% O₂) was abrogated by HIF-1 α siRNA but not by HIF-2 α or non-targeting (NS) siRNA ($p < 0.001$). These data indicate that enhanced upregulation of GLS in hypoxic conditions occurs in an HIF-1 α dependent manner.

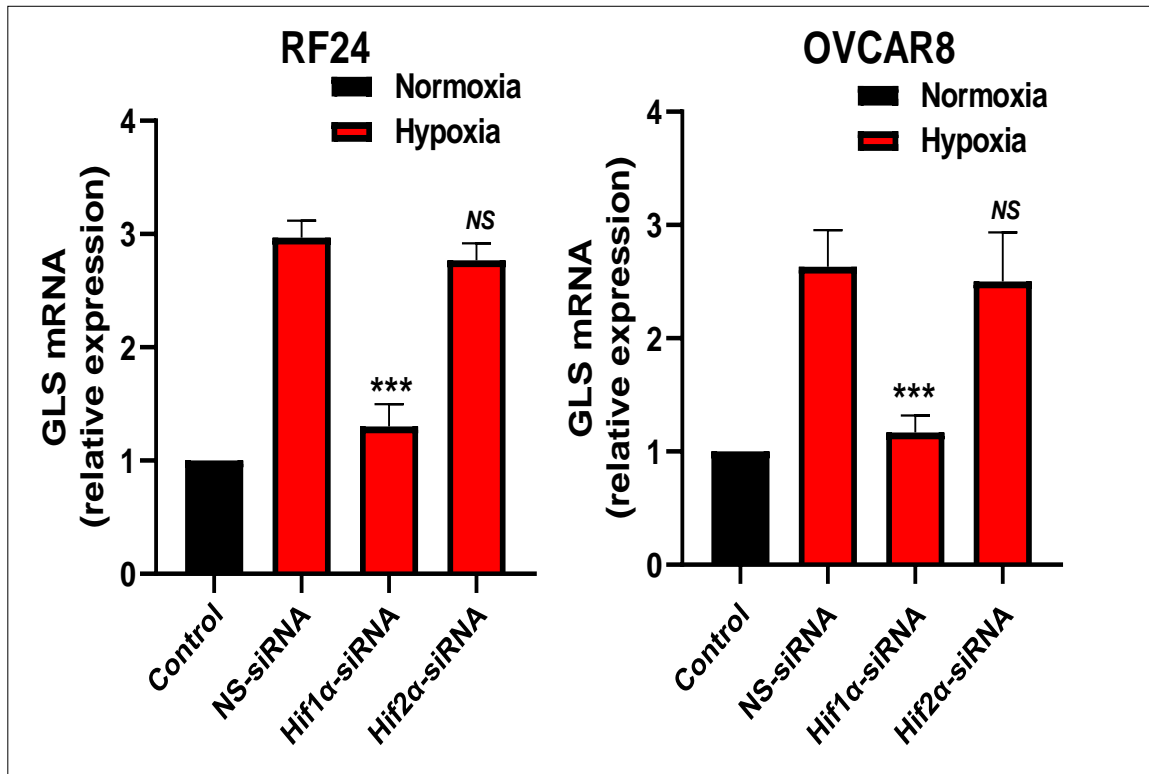


Figure 18. Effect of HIF-1 α on GLS expression. RF24 and OVCAR8 cells were transfected with HIF-1 α or HIF-2 α siRNA following exposure to 1% O₂ for 24 hours. GLS mRNA relative expression was then quantified and was significantly reduced with HIF1 α -siRNA but not with HIF2 α -siRNA. Non-targeting siRNA (NS-siRNA) were used for control. Error bars, SEM, *** $p < 0.001$. NS, non-significant.

GLS is ubiquitously expressed in both ovarian cancer and endothelial cell lines

Before performing additional *in vitro* experiments to assess the effects of GLS inhibition on ovarian cancer and endothelial cell lines, we first confirmed GLS expression in eight ovarian cancer cell lines, including A2780, HeyA8, SKOV3, OVCAR3, OVCAR4, OVCAR5, OVCAR8, and IGROV (Figure 19A). After culturing the cells under normoxic conditions, GLS expression levels were noted to be highest in the SKOV3 cells; therefore, we chose this cell line for further *in vivo* work. A similar

GLS expression level to the SKOV3 cell line was observed in the parental line of endothelial cells (RF24) as well as endothelial cells with an acquired resistance to AVA therapy with bevacizumab (RF24-bev, Figure 19B). Therefore, the RF24 and RF24-bev cell lines were chosen to be utilized for additional *in vitro* investigations.

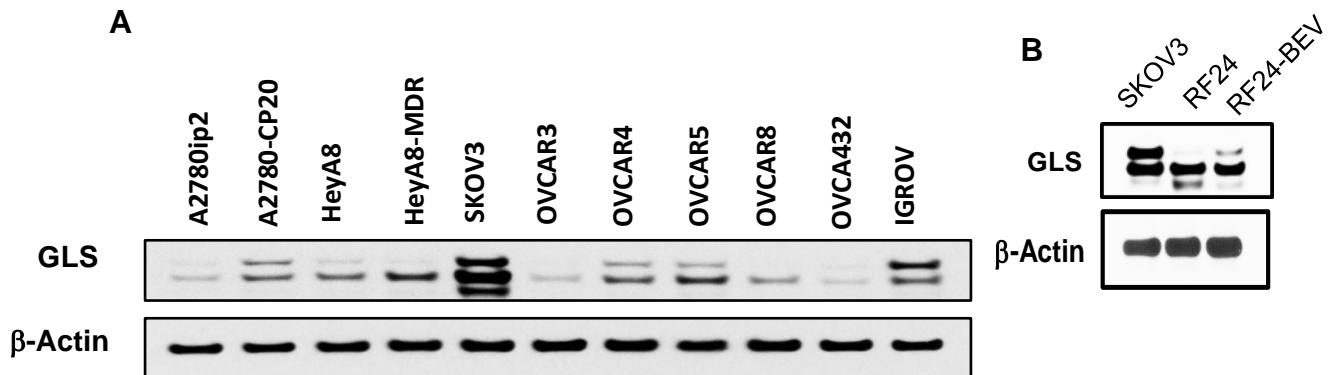


Figure 19. Baseline GLS expression levels in ovarian cancer and endothelial cells. (A) Western blot of GLS expression level in multiple untreated ovarian cancer cell lines. **(B)** Western blot of GLS expression in SKOV3 ovarian cancer cells and in both a parental and bevacizumab-resistant endothelial cell line (RF24 and RF24-Bev, respectively).

Altered glutamine metabolism under hypoxic conditions enhances sensitivity to GLS inhibition for both ovarian cancer and endothelial cells in vitro

After establishing that there was a high GLS expression in ovarian cancer cell lines and that glutaminolysis was increased after the hypoxic stress imposed by AVA treatment, we next targeted the increased reliance on glutamine as a potential vulnerability. We did so with an internally synthesized glutaminase inhibitor (GLSi) known as IACS-012031, subsequently referred to as GLSi throughout the text. This

compound possesses the same chemical structure as the commercially available and clinically tested GLS inhibitor called CB-839.^{43,49}

First, the viability of OVCAR5, OVCAR8, and SKOV3 cells after culturing with escalating doses of this GLSi was tested *in vitro*. Under normoxic conditions, the viability of all three cell lines was inhibited in a time-dependent manner with a 30-60% reduction in viability compared to untreated control cells (Figure 20A). Culture of the parental RF24 endothelial cell line with AVA, GLSi, or both demonstrated a greater reduction in cell viability when treated with GLSi as monotherapy compared to AVA monotherapy under normoxic conditions, an effect that was even more pronounced when the AVA and GLSi treatments were combined (36% vs 61% vs 6.3%, respectively; Figure 20B). Parental (RF24 par) and bevacizumab-resistant RF24 (RF24-bev) cells demonstrated a dose-dependent inhibition of viability, with the resistant cells exhibiting greater sensitivity to GLSi-based therapy than the parental cells (Figure 20C). Specifically, the viability of the RF24-Bev cells was about 50% lower than that of RF24-par cells when cultured under hypoxic conditions with the same dose of GLSi, with median half-maximal inhibitory concentrations (IC_{50}) of GLSi of 63.2 nM in RF24-par cells and 33.1 nM in RF24-Bev cells (Figure 20C).

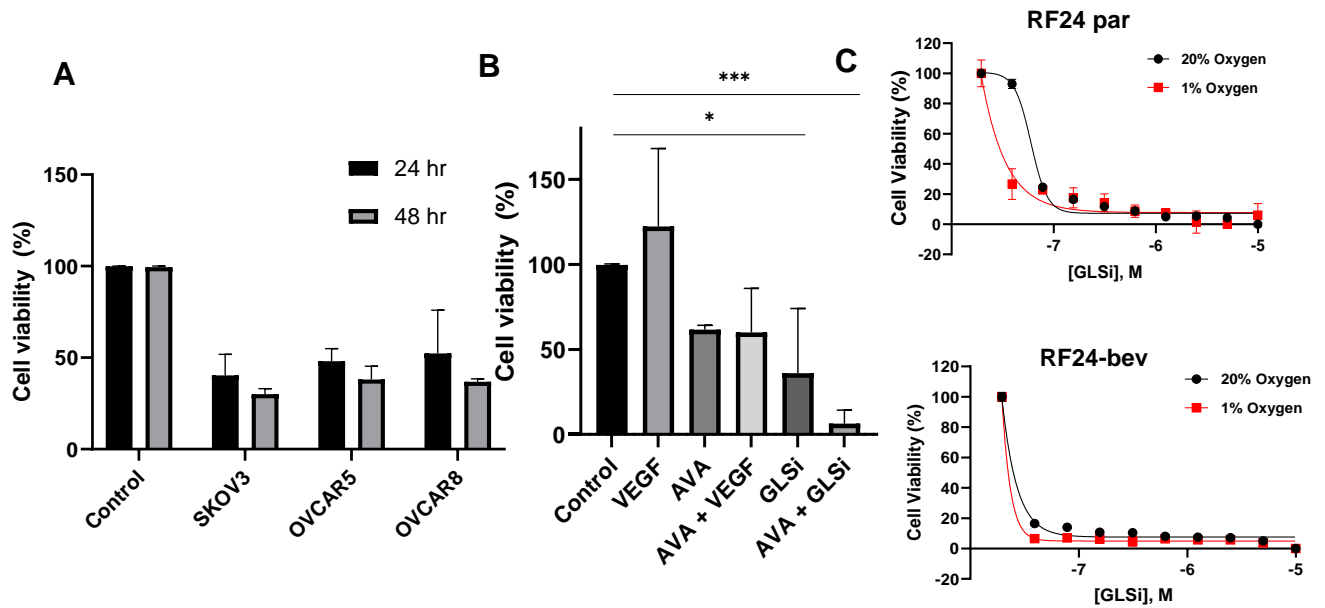


Figure 20. Hypoxia enhances sensitivity to GLS inhibition in both cancer and endothelial cells in vitro. (A) The viability of three ovarian cancer cell lines (SKOV3, OVCAR5, and OVCAR8) upon culture with GLSi [1.0 μ M] monotherapy for 24-48 hours ($p < 0.05$). **(B)** The viability of the RF24-par endothelial cell line after culturing with AVA or GLSi monotherapy or a combination of both therapies for 24 hours in normoxic conditions ($*p < 0.05$, $***p < 0.001$). Positive control: VEGF. **(C)** The viability of RF24-par and bevacizumab-resistant RF24 cells (RF24-bev) after culture in increasing concentrations of GLSi in either normoxic (20% O₂, black line) or hypoxic (1% O₂, red line) conditions.

Next, the angiogenic capability of the cells was assessed *via* a tube formation assay with the RF24 endothelial cells which were cultured with GLSi for six hours (Figure 21A and B). Under normoxia, the combination of GLSi and AVA resulted in significantly less tube formation than did monotherapy with either drug (branch count 9.2 vs. 21.0 and 13.2, respectively; $p < 0.01$) or no treatment (control 27.4; $p <$

0.001). This effect of reduced tube formation ability was even more pronounced in hypoxia than in normoxia, again demonstrating that GLSi in combination with AVA had a significantly greater reduction in tube formation than control therapy or monotherapy with either GLSi or AVA (2.6 vs. 16.8, 14.9, and 8.2, respectively; $p \leq 0.001$). Ultimately, we observed increased sensitivity of both ovarian cancer and endothelial cell lines to GLSi therapy under hypoxic conditions, an effect that was even more pronounced when GLSi was combined with AVA, and particularly when treating the endothelial cells that were resistant to AVA.

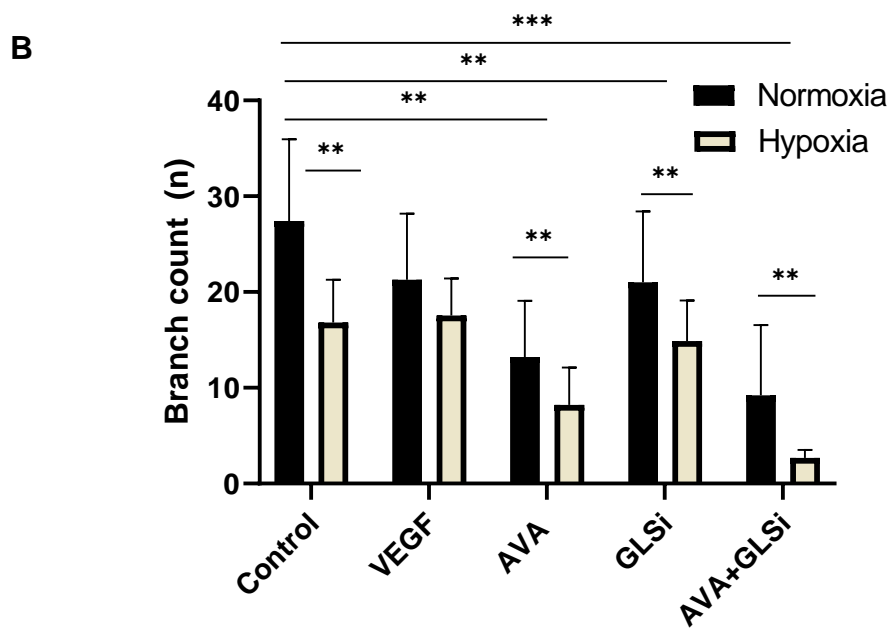
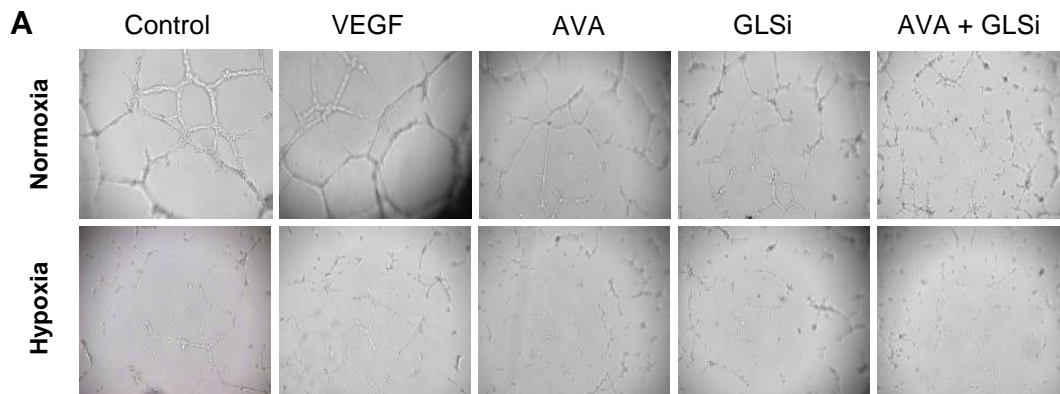


Figure 21. Assessment of angiogenic potential of cells upon culturing with AVA and GLSi in normoxic and hypoxic conditions. (A) Bright field microscopic images at 50X showing the vessel loop formation and the effect of bevacizumab (AVA) and GLSi monotherapy or in combination (AVA + GLSi) on the angiogenic capability of RF24-par cell cultures in normoxia (20% O₂) versus hypoxia (1% O₂). **(B)** Average branch counts of the vessel loops described in **(A)** detected at 6 hours as measured in triplicate experiments; ** $p < 0.01$, *** $p < 0.001$. VEGF, vascular endothelial growth factor; AVA, anti-VEGF antibody; GLSi, glutaminase inhibitor.

GLSi has robust antitumor effects in combination with AVA in vivo

To further validate the *in vitro* findings of increased GLSi sensitivity in hypoxia for both ovarian cancer and endothelial cells, we performed an *in vivo* experiment with an orthotopic SKOV3ip1 ovarian cancer mouse model. In this experiment, we randomized 60 nude mice to receive treatment with a vehicle control, AVA, GLSi, or a combination of AVA and GLSi given at the same doses as in monotherapy (Figure 22).

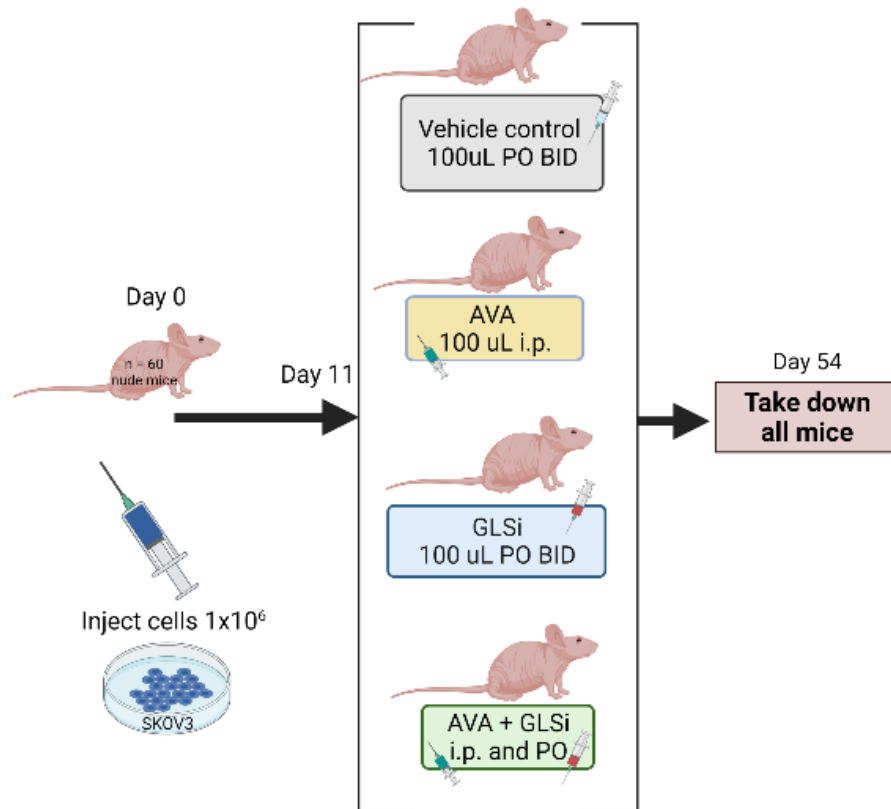


Figure 22. Experimental plan to investigate the efficacy of GLSi in vivo. Schema of the *in vivo* experiment investigating the efficacy of GLSi treatment as monotherapy or in combination with AVA treatment as compared to a vehicle control.

After seven weeks of treatment, the group of mice treated with the combination of AVA and GLSi exhibited a robust antitumor effect as clearly seen on gross necropsy (Figure 23) as well as quantifiably with a lower mean tumor weight (0.05 g vs. 0.62 g and 0.64 g; $p < 0.01$) and tumor nodule number (3.3 vs. 12.8 and 13.9; $p < 0.05$) than those in the control and GLSi monotherapy groups, respectively (Figure 24 A and B).

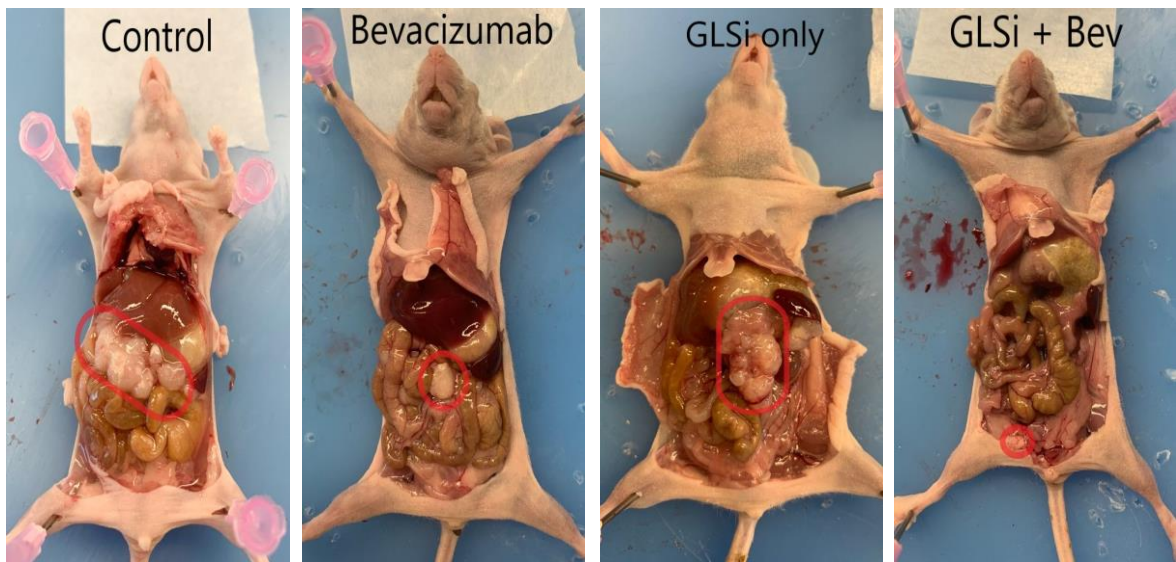


Figure 23. Robust antitumor effect of GLSi combined with AVA as assessed using gross necropsy. Gross inspection of tumor volume in an SKOV3ip1 mouse model after either no treatment (Control), bevacizumab (AVA), GLSi, or a combination of bevacizumab and GLSi (GLSi + Bev). Tumor nodules are circled in red outline. AVA, anti-VEGF antibody; GLSi, glutaminase inhibitor; Bev, bevacizumab.

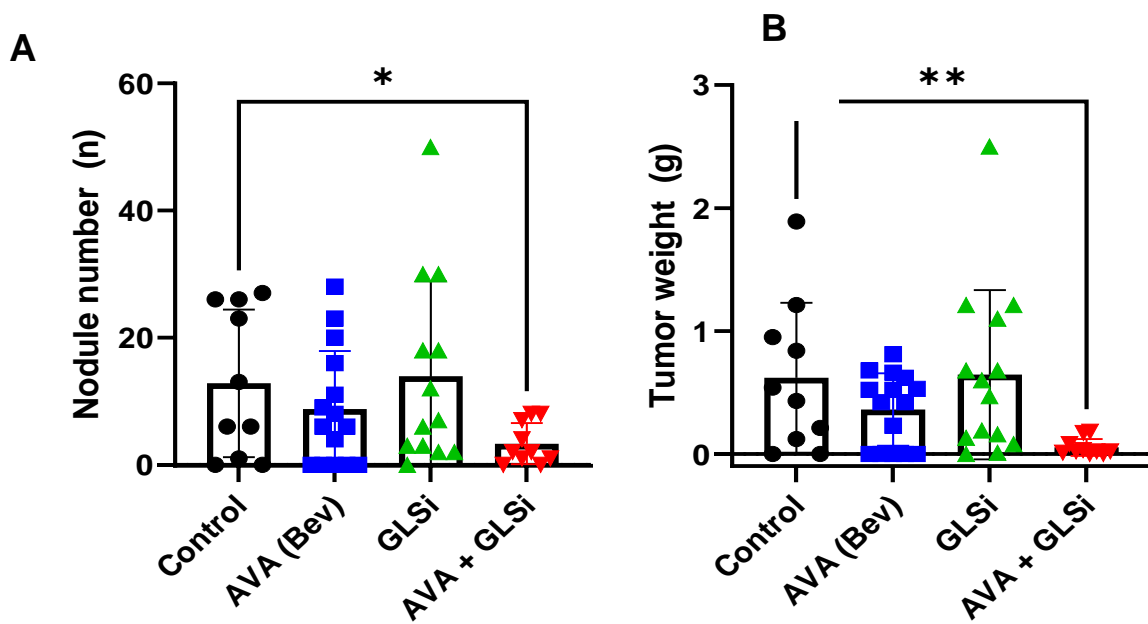


Figure 24. Effect of GLSi combined with AVA on tumor burden in an SKOV3ip1 mouse model at time of gross necropsy. (A) Nodule numbers and (B) tumor weights of SKOV3ip1 mouse model after either no treatment (Control), AVA, GLSi, or a combination of AVA and GLSi. Error bars, SD. * $p < 0.05$; ** $p < 0.01$ (compared with the control group using the Student t -test). AVA, anti-VEGF antibody; GLSi, glutaminase inhibitor; Bev, bevacizumab.

The mean body weights were not significantly different between the combination therapy, GLSi monotherapy, and control groups (23.6 g, 22.0 g, and 22.1 g, respectively; $p = 0.16$, Figure 25).

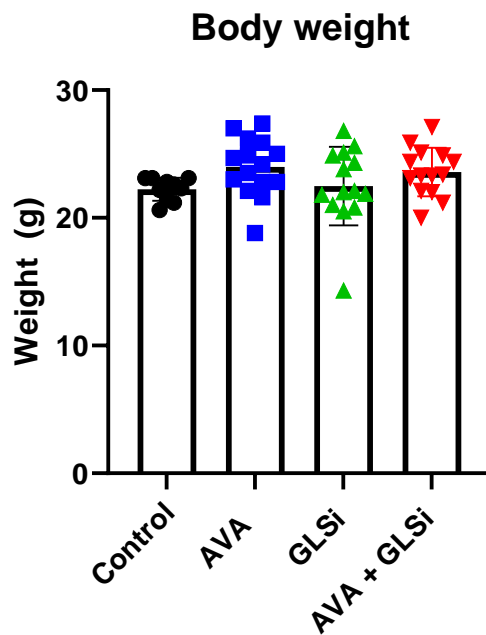


Figure 25. Mouse body weight after treatment with AVA, GLSi or combination therapy. Body weights of SKOV3ip1 mouse model after randomization and treatment into one of four groups: control, AVA, GLSi, or combination of bevacizumab plus GLSi therapy (AVA + GLSi); $p = 0.16$. AVA, anti-VEGF antibody; GLSi, glutaminase inhibitor.

The mean tumor vessel density, as assessed by IHC staining for the endothelial cell marker CD31, in the combination therapy group was lower than in the control, GLSi monotherapy, and AVA monotherapy groups (11 vs. 30, 15, and 15, respectively; $p < 0.001$, Figure 26A). The tumors in the combination group also exhibited less cell proliferation than those in the GLSi and AVA monotherapy

treatment groups or control groups, respectively, as assessed using Ki67 staining (mean cell count/hpf: 108 vs. 151, 200, and 292; $p < 0.01$, Figure 26B).

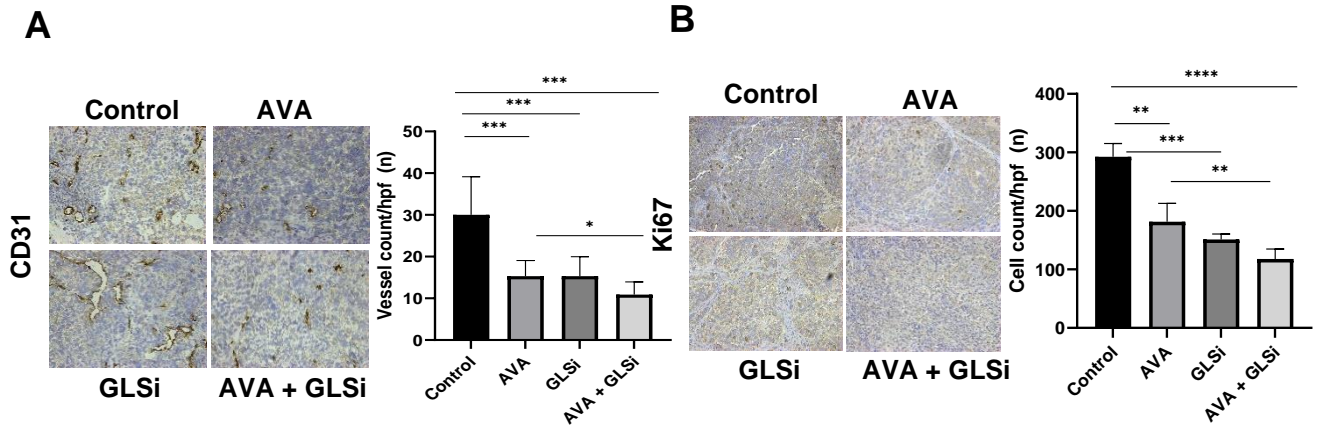


Figure 26. Immunohistochemistry analysis of vascular density and cellular proliferation after treatment with AVA, GLSi or combination therapy. (A) Blood vessel densities in ovarian tumor tissues harvested from mice in each treatment group as assessed by endothelial cell marker CD31, $*p < 0.05$; $***p < 0.001$. **(B)** Cell proliferation assay according to immunohistochemistry staining of mouse ovarian cancer tissues with anti-Ki67, $** p < 0.01$, $***p < 0.001$, $****p < 0.0001$. AVA, anti-VEGF antibody; GLSi, glutaminase inhibitor.

A subset of tissues obtained from this experiment ($n = 5$ per treatment group) were also subjected to DESI-MS imaging analysis to investigate treatment-specific alterations. The relative abundances of 74 features were significantly altered among treatment groups, corresponding to a broad range of small metabolites and lipid species (Figure 27, FDR $< 5\%$).

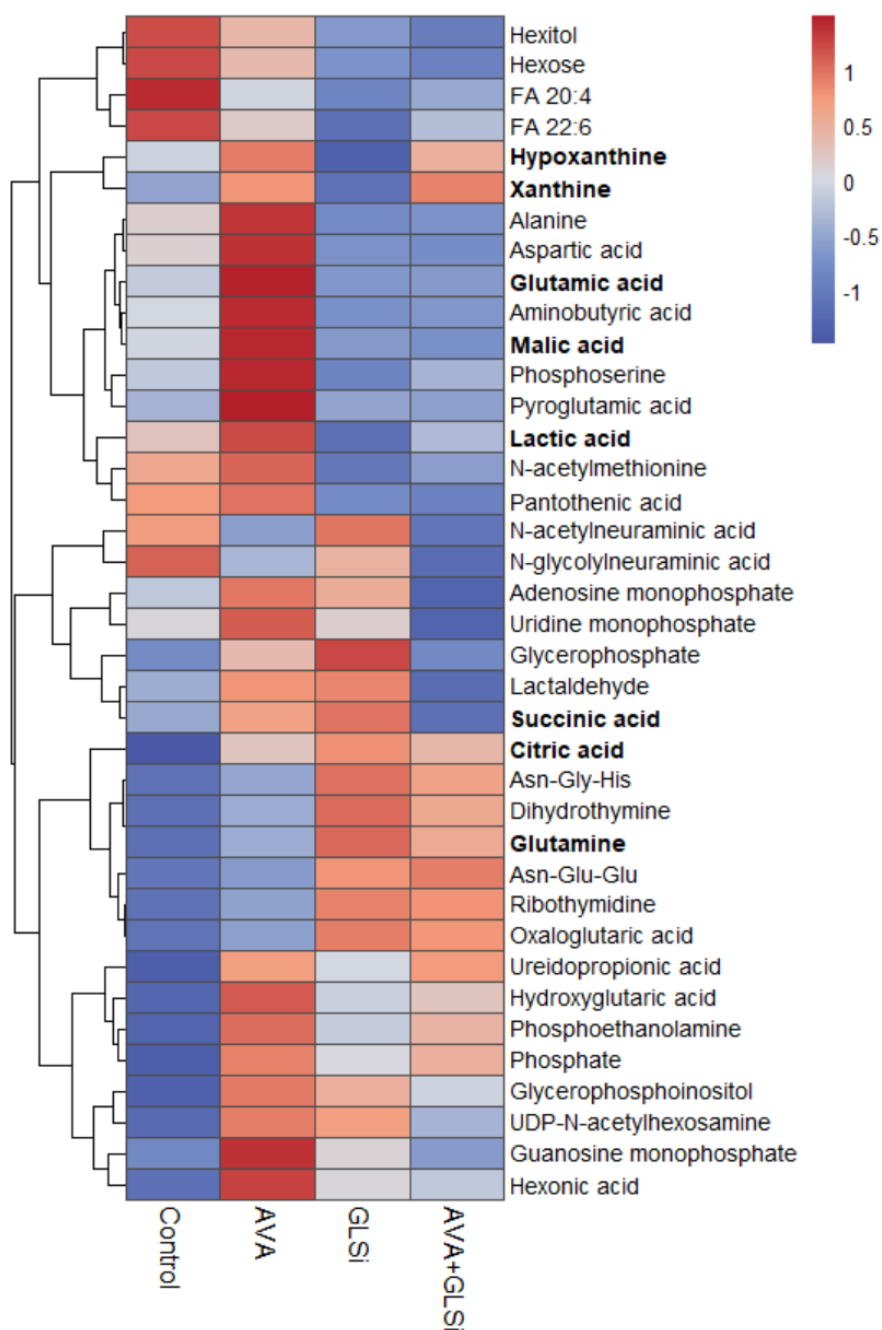


Figure 27. Heat map of altered metabolites seen after treatment with AVA and GLSi mono- and combo-therapy. Intensity heat map for metabolites selected by SAM as significantly altered among SKOV3ip1 tumors treated with a vehicle control, AVA, GLSi, or AVA + GLSi (FDR < 5%) identified by DESI-MS imaging. Features were clustered using a Euclidean-distance formula according to the average signal intensity of the

corresponding m/z value measured from tumor-specific regions. The color scale reflects z-score standard deviations from the mean relative abundance measured for each ion. For fatty acid (FA) species, X:Y indicates the number of carbons and double bonds, respectively.

In particular, an overall reduction in the relative abundances of glutamate, malate, and hexose were identified in the combination therapy group compared to the control or monotherapy groups with either GLSi or AVA, respectively (normalized ion abundance of glutamate: 9.2, 13.1, 11.2 vs. 16.3, respectively; $p < 0.05$, Figure 28). The relative abundances of glutamine and citrate were significantly increased in the GLSi monotherapy and combination groups compared to the control and AVA monotherapy groups (normalized ion abundance of glutamine: 13.4 and 9.0 vs. 1.9 and 3.6, respectively $p < 0.0001$, Figure 28).

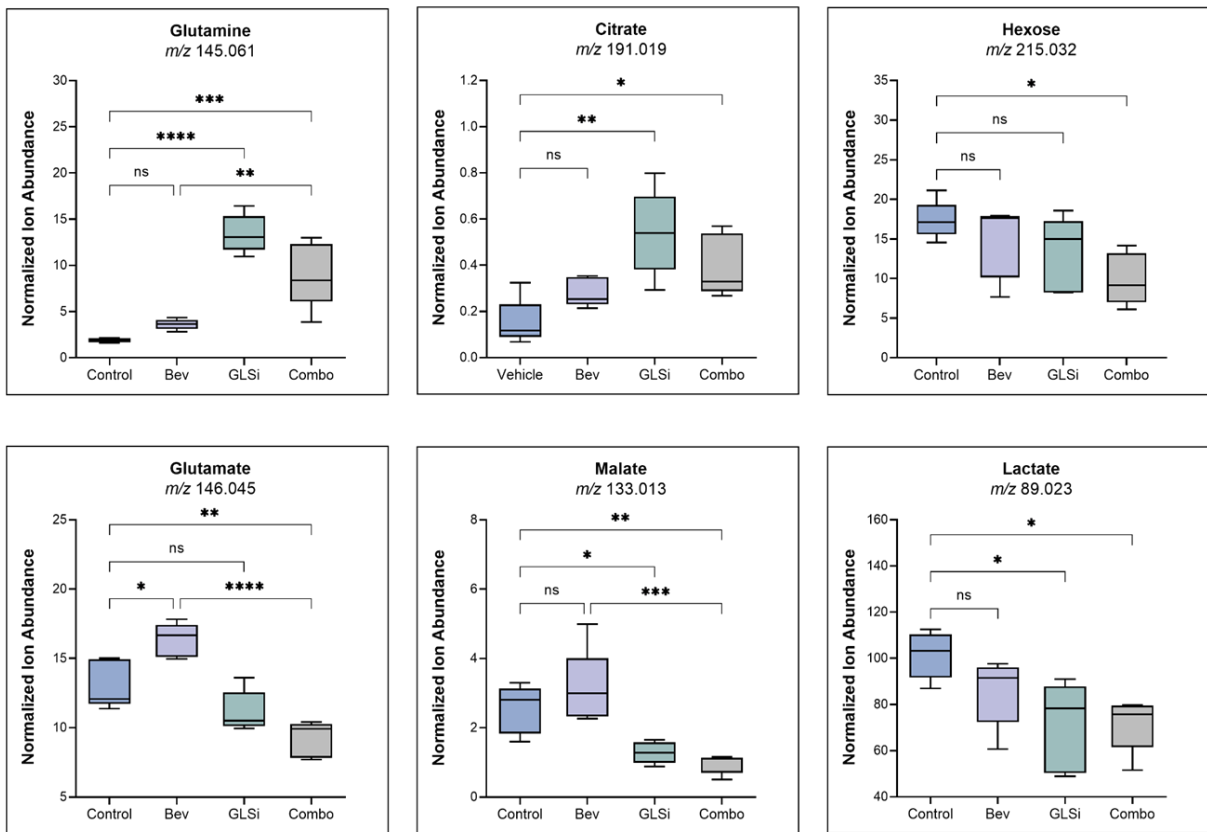


Figure 28. Normalized ion abundance of key metabolites after combination therapy with GLSi and AVA treatment. Median normalized intensity of the relative abundance of glutamate metabolism and TCA cycle intermediates in control, AVA (Bev) monotherapy, GLSi monotherapy, and combination therapy groups (Combo) mice in the SKOV3ip1 orthotopic ovarian cancer model. * $p < 0.05$, ** $p < 0.01$, *** $p < 0.001$, **** $p < 0.0001$. AVA, anti-VEGF antibody; Bev, bevacizumab.

When evaluating the conversion of pyruvate to lactate in the treatment groups, we observed a reduced relative abundance of lactate relative to pyruvate in all treatment groups compared to control, this was most notable in the GLSi monotherapy and combination therapy groups, suggesting that the most substantial

impact arising from GLSi therapy is on lactate metabolism (ion abundance of lactate: 70.9, 72.6, 85.7 vs. 101.4, $p < 0.05$, Figure 29 A and B). As expected, we observed an overall reduction in the ratio of glutamine to glutamate conversion after GLSi monotherapy and this reduction was sustained after combining GLSi with AVA treatment (Figure 29 C). Moreover, the effect of reduced glutaminolysis observed with GLSi and AVA combination therapy was more profound than the reduction we observed in the AVA monotherapy of the AVA-sensitive tumor tissues (as seen in Figure 16), suggesting that targeting both angiogenesis and the hypoxic adaptations from it with both AVA and GLSi therapy significantly altered the tumor metabolism.

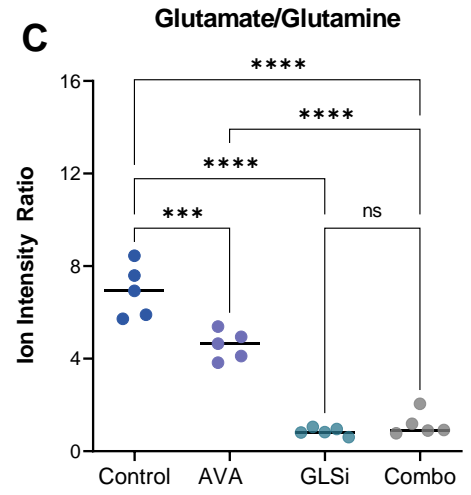
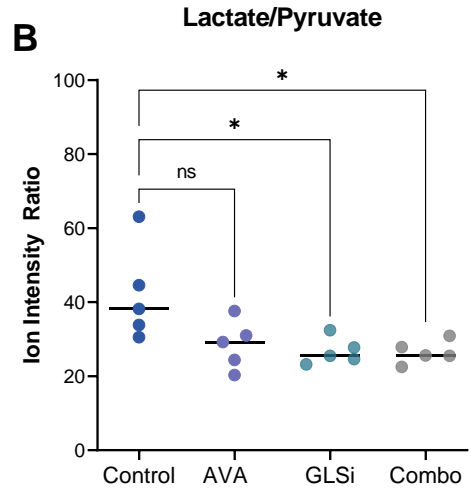
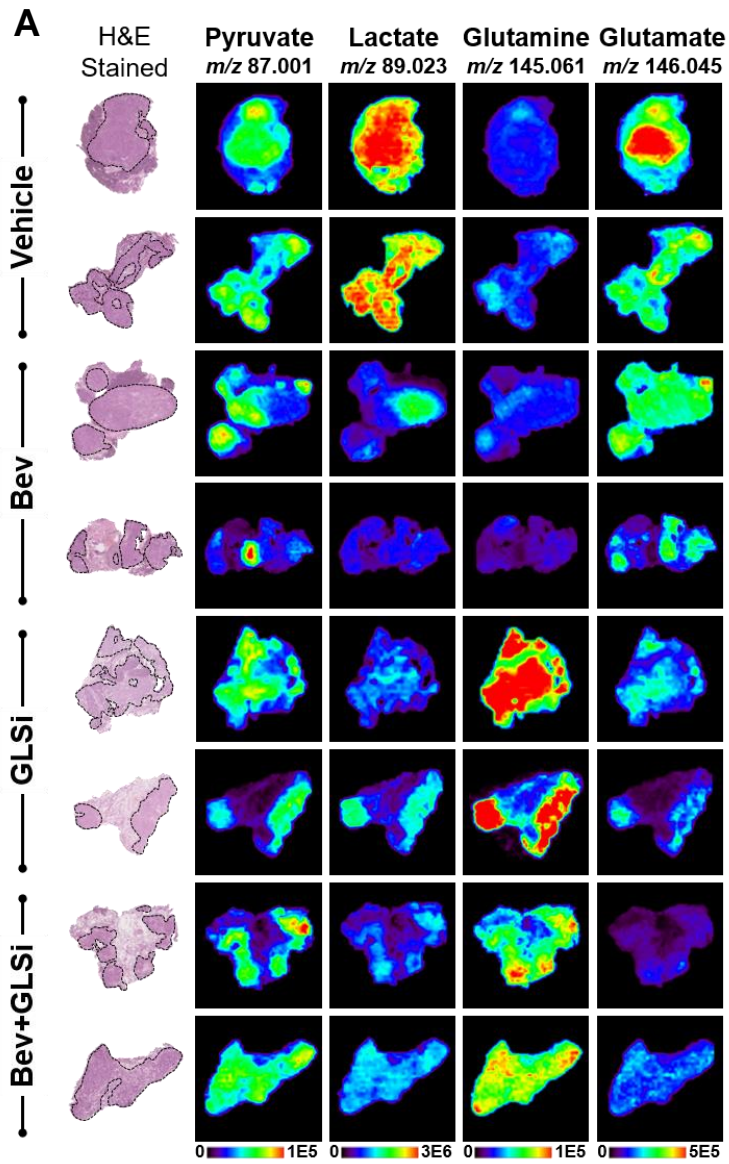


Figure 29. DESI-MS ion images of ovarian tumors after treatment with either AVA, GLSi, or combination therapy. (A) Representative DESI-MS ion images of pyruvate, lactate, glutamine, and glutamate in mouse tumors after treatment with a vehicle control, AVA, GLSi, or a combination of the two. H&E, hematoxylin and eosin. **(B)** Median normalized intensity of the lactate to pyruvate ratio in the control and treatment groups. * $p < 0.05$; ns, not significant. **(C)** Median normalized intensity ratio of glutamate to glutamine in the control, AVA monotherapy, GLSi monotherapy and combination therapy treatment groups. Statistical significance was determined by Tukey's HSD test, *** $p < 0.001$, **** $p < 0.0001$. Bev, bevacizumab anti-VEGF antibody; GLSi, glutaminase inhibitor; ns, not significant.

Detection of GLSi therapy response using hyperpolarized magnetic resonance spectroscopy

To further assess the therapeutic efficacy of GLSi therapy using a non-invasive approach, we performed hyperpolarized magnetic resonance spectroscopy (HP-MRS) to quantify any metabolic changes in pyruvate-to-lactate metabolism associated with this therapy in real-time. We did so using a total of 10 mice from the aforementioned SKOV3ip1 model of adaptive resistance of ovarian cancer to AVA therapy, with five mice receiving a vehicle control and five receiving GLSi. HP-MRS is a novel technique that enhances the sensitivity of traditional magnetic resonance imaging (MRI) up to 10,000-fold and facilitates a direct, non-invasive analysis of the flux of pyruvate metabolism with spatial resolution of tumors *in situ*.⁶⁶ Baseline MRI

images were obtained with mice under anesthesia to confirm tumor location in both groups. After tail vein injection of hyperpolarized [1-¹³C] pyruvate as outlined in the Materials and Methods, we quantitatively calculated each tumor's normalized lactate over pyruvate ratio, defined as the ¹³C resonance signal of lactate divided by the ¹³C resonance signal of pyruvate over 60 seconds. Our analysis demonstrated that pyruvate-to-lactate conversion in AVA-resistant tumors was significantly reduced *in vivo* by GLSi therapy (0.337 vs. 0.178; $p \leq 0.001$, Figure 30A, B). These findings are concordant with the changes in relative abundance measured for pyruvate and lactate using DESI-MS imaging in the experiment discussed above (Figure 29B). This suggests that HP-MRS real-time imaging provides an early identification of treatment effect from GLSi therapy.

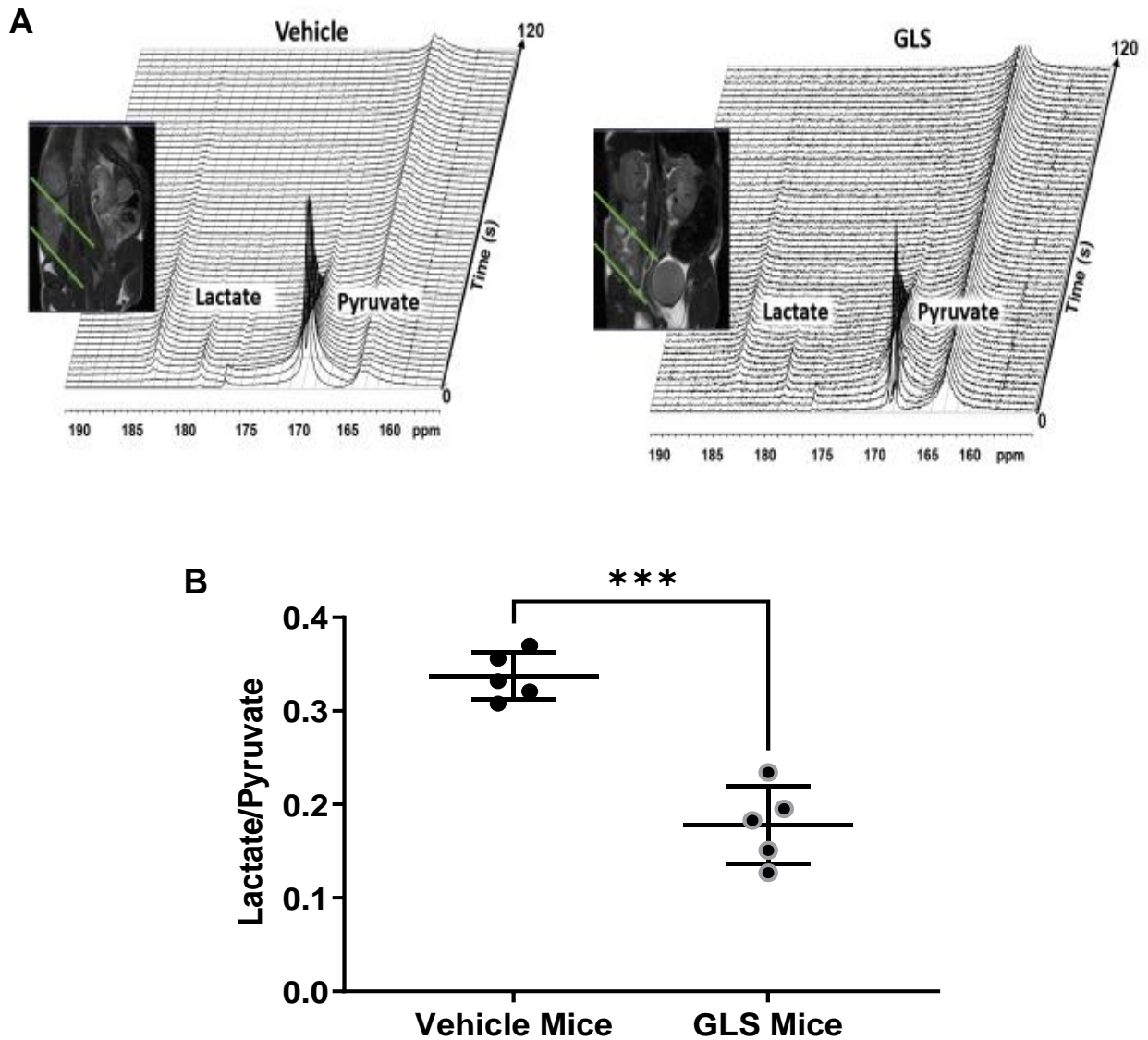


Figure 30. Detection of GLSi therapy response by HP-MRS. (A) Representative T2-weighted MRI (coronal slice) and real-time in vivo ^{13}C magnetic resonance spectroscopy images of AVA-resistant ovarian tumors in mice after intravenous hyperpolarized pyruvate injection for two treatment groups: vehicle control (left) and GLSi (right) with spectra collected from the MRI slabs on the ovarian tumors over two seconds. **(B)** The normalized lactate/pyruvate ratios for vehicle- and GLSi-treated mice. $***p < 0.001$. GLS, glutaminase targeted treatment.

GLS inhibition at the emergence of AVA resistance restores sensitivity in an adaptive resistance model of ovarian cancer

After observing the robust antitumor effects of GLSi combined with AVA therapy when given in combination up-front, we set out to determine whether GLSi could restore sensitivity of ovarian cancer to AVA therapy if initiated after AVA-resistance was established. For this experiment, we again used the SKOV3ip1 orthotopic mouse model but administered AVA monotherapy with bevacizumab after tumor establishment and continued it until resistance was confirmed by bioluminescence imaging (Figure 31).

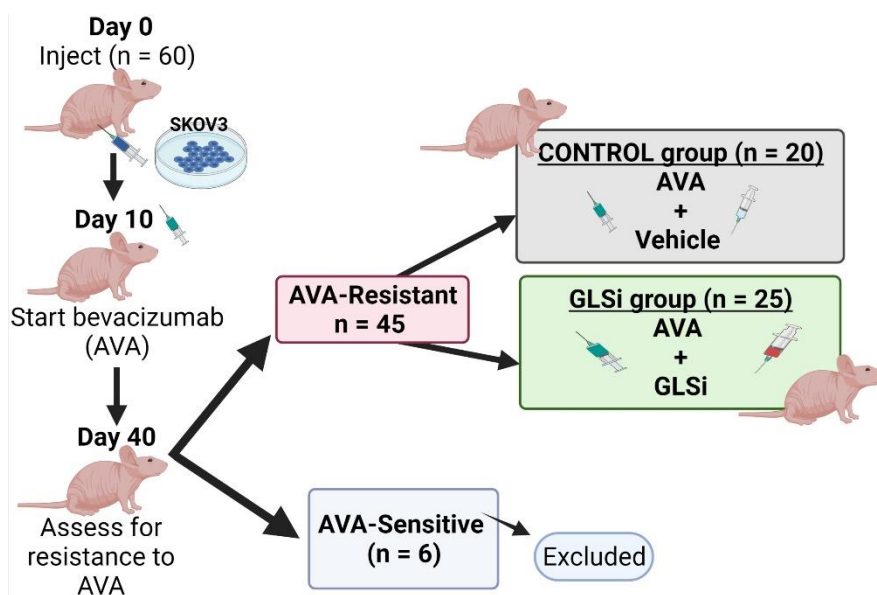


Figure 31. Experimental plan to evaluate if AVA resistance can be restored with GLSi therapy. Schema of the orthotopic SKOV3ip1 mouse model in which AVA-resistance was established prior to the initiation of GLSi therapy. AVA, anti-VEGF antibody (bevacizumab); GLSi, glutaminase inhibitor.

After AVA-resistance was observed, we excluded the AVA-sensitive mice and maintained all AVA-resistant mice on AVA therapy. We subsequently randomized them to receive either a vehicle control or GLSi (both at 200 μ L *via* oral gavage twice a day) until they became moribund. Initiation of GLSi therapy after establishment of adaptive resistance to AVA therapy resulted in a partial abrogation of tumor growth as evidenced by a 57% reduction in mean tumor weight (0.43 g vs. 1.01 g; $p = 0.04$) and a 68% lower mean tumor nodule number in the GLSi group than in the control group (5 vs. 15; $p = 0.0003$, Figure 32).

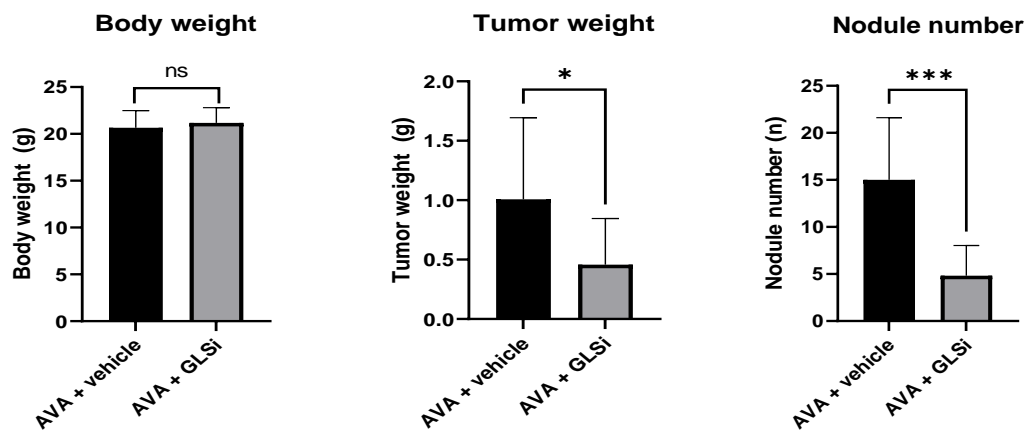


Figure 32. AVA sensitivity is restored when GLSi therapy is administered after AVA resistance is established. Mouse body weights, tumor weights, and nodule numbers at the time of gross necropsy for mice treated with AVA combined with a vehicle vs. those given AVA combined with GLSi. Error bars, SD. * $p < 0.05$; *** $p < 0.001$ (compared with the control group using the Student *t*-test). AVA, anti-VEGF antibody; GLSi, glutaminase inhibitor; ns, not significant.

The administration of GLSi therapy after the emergence of AVA resistance not only provided an anti-tumor response, but it also resulted in a significant survival benefit (median survival 69 vs. 65 days; $p = 0.04$). Continuing AVA therapy in the resistant setting with a vehicle control was associated with a twofold increased risk of death compared to treatment with AVA plus a GLSi (HR 2.069; 95% CI 1.03 - 4.15; Figure 33). We observed treatment toxicity in the AVA plus GLSi treatment group, as evidenced by weight loss in this treatment group during the experiment. However, mouse weight recovered with dose adjustments and was not significantly different among the groups at the conclusion of the study (see Figure 32, left panel). Our dose reduction mirrored a standard dose reduction protocol used in humans whereby treatment was held for 48-72 hours after recognition of weight loss and the dose was subsequently resumed at 2/3 the starting dose. In this experiment, the starting dose was 200 μ L of GLSi given via oral gavage twice daily (BID). The reduced dose was therefore 200 μ L every morning and 100 μ L in the evening.

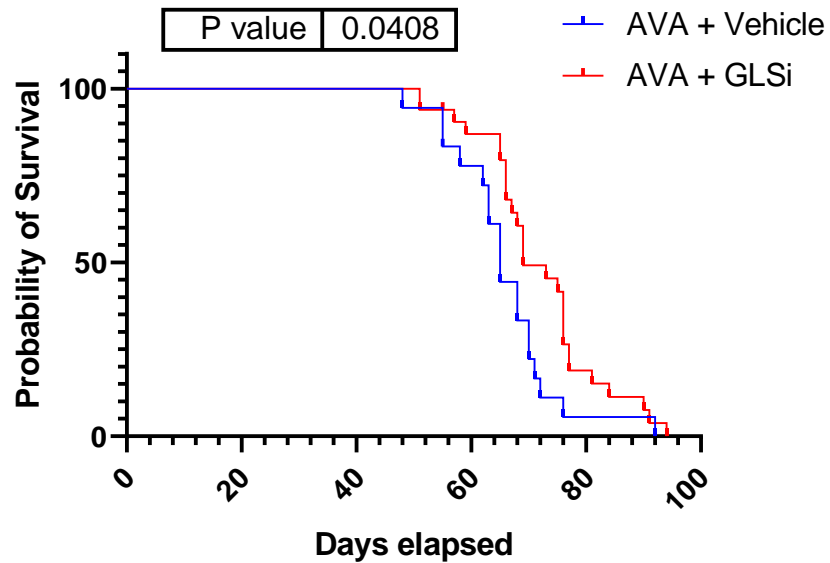


Figure 33. Kaplan-Meier survival curve showing survival advantage with GLSi therapy after AVA resistance is established. Nude mice were inoculated with the SKOV3ip1 cell line and treated with AVA therapy until an adaptive resistance to it emerged. Following AVA-resistance, the mice were continued on AVA therapy and randomized to add on either a vehicle control or GLSi therapy. GLSi therapy resulted in a survival advantage compared to vehicle control ($p = 0.0408$). Continued therapy with AVA and a vehicle control was associated with a twofold increase risk of death compared to AVA plus GLSi therapy (HR 2.069; 95%CI 1.03 – 4.15). AVA, anti-VEGF antibody; GLSi, Glutaminase inhibitor.

DISCUSSION

Key Findings

Overall, the key finding of our investigation is that increased glutamine metabolism is a metabolic adaptation to hypoxia that occurs in response to resistance to AVA therapy in an orthotopic mouse model of ovarian cancer. We exploited this metabolic vulnerability of glutamine dependence by combining AVA therapy (bevacizumab) with GLSi which produced robust antitumor efficacy in both *in vitro* and *in vivo* models of ovarian cancer.

Glutamine metabolism and regulation in response to AVA therapy *in vitro*

Reliance on glutamine metabolism for growth and development is an established hallmark of cancer.²² However, the fate of glutamine and its metabolism is complex.⁶⁷ Previously, our lab reported the adaptive nature of the TME under nutrient stress, and in particular, elucidated the role of reactive stromal cells under glutamine deprivation and the ability of malignant tumors to harness carbon and nitrogen from alternative sources to maintain glutamine stores.⁶⁸ Use of these glutamine stores is heterogeneous, as they can be consumed during protein synthesis, serve as building blocks for the antioxidant glutathione, or be converted into α -ketoglutarate for TCA cycle anaplerosis via glutaminase (GLS).^{37,67} The role of GLS in cancer growth and progression varies among human cancers and is dependent on the cancer phenotype, with strong evidence of an oncogenic role for GLS in colon, liver, and ovarian cancers but not in other cancers, such as non-small cell lung cancer.⁶⁷ Thus, GLS expression and the prognostic implications of its

expression vary by cancer type, with higher GLS expression associated with worse prognosis for ovarian cancer.⁶⁴

Here we confirmed that GLS is ubiquitously expressed in a panel of ovarian cancer cell lines and that hypoxia is positively correlated with GLS expression level. Furthermore, we identified that one of the metabolic adaptations exhibited by both ovarian cancer cells and endothelial cells *in vitro* after treatment with AVA therapy is an upregulation of GLS expression. Moreover, we observed that this GLS expression is regulated in an HIF-1 α dependent manner. Further work is needed to identify the transcription factor(s) and or promoters involved to determine whether this effect is direct or indirect. However, given the well-documented association between the hypoxic stress imposed by anti-angiogenic therapy and the increased expression of HIF-1 α ²³, these *in vitro* findings support the biologic plausibility of an increased efficacy of targeted therapy with AVA when combined with a GLS inhibitor. In fact, when we utilized a GLSi to target the hypoxia-mediated increase in GLS expression after AVA treatment *in vitro*, we observed a significant vulnerability. This was particularly the case in the AVA-resistant endothelial cell line, RF24-Bev.

Metabolic adaptations observed in AVA resistance

Using both LC-MS and DESI-MS we identified a number of metabolic adaptations that occur in response to AVA treatment, and specifically after adaptive resistance to it. The predominant changes were consistent across the LC-MS and DESI-MS modalities as we noted a global upregulation of purine metabolism in the AVA-resistant tumors compared to control tumors in both. Specifically, the metabolites such as urate, xanthine, hypoxanthine, xanthosine and 3-

ureidopropionate were higher in the AVA-resistant group, compared to control tumors. Given that glutamine is a required substrate for de novo synthesis of these purine nucleotides,⁶⁹ these findings support the hypothesis that blunting glutaminolysis by inhibiting the GLS enzyme would be tumoricidal. When we evaluated the AVA-resistant tumors with DESI-MS, we saw an increased expression of glutamate relative to glutamine, further suggesting that GLS inhibition is a potential vulnerability in AVA-resistance that could be targeted.

Examination of up-front combined therapy with GLSi and AVA with *in vivo* models

We sought to validate the *above in vitro* observations with a series of *in vivo* experiments. We first assessed the efficacy of GLSi therapy when given up-front in combination with AVA therapy, prior to the emergence of AVA-resistance in a mouse model of ovarian cancer. We noted a profound antitumor effect of GLSi in the SKOV3ip1 ovarian cancer orthotopic mouse model. Upon DESI-MS analysis of the tumor tissues from this experiment, we observed a significant decrease in anaerobic metabolism and glutaminolysis as noted by an increased abundance of both pyruvate and glutamine in the tissues obtained from mice treated with GLSi monotherapy or combination therapy with GLSi and AVA. These findings were not observed in the AVA monotherapy group but seen in the GLSi monotherapy and, more strongly, in the combination of AVA and GLSi therapy. Taken together, this suggests that it is the GLSi therapy, not AVA treatment, that is responsible for the observed changes in the anaerobic metabolism of these tumors. Therefore, we observed that GLSi therapy impacts the glutaminolysis pathway and has a more

global effect on tumor metabolism, particularly when given in combination with AVA therapy up-front, prior to AVA-resistance.

Assessment of the ability of GLSi to restore sensitivity to AVA therapy

Given the robust treatment response observed with up-front therapy, we next set out to investigate whether GLSi therapy could restore sensitivity to AVA treatment after AVA-resistance is established. This arena of therapy represents a critical unmet need in the clinical setting. The reality is that nearly every patient treated for ovarian cancer will be exposed to AVA therapy with bevacizumab at some point along their cancer care journey because of its broad FDA approvals for first-line treatment for treatment in the recurrent or maintenance setting.^{14,25,27} As we described, however, adaptive resistance to therapy develops nearly universally within months of initiation of treatment and additional agents are needed to target this population of patients with AVA-resistant disease.

In our established orthotopic mouse model of AVA-resistant disease⁵⁹ where 80-90% of the mice receiving AVA treatment demonstrate an adaptive resistant to it, we investigated the utility of GLSi therapy. Our results demonstrate a profound antitumor efficacy of GLSi therapy administered in this setting with a reduction in tumor burden by nearly a third. This was associated with a statistically significant survival benefit. Similarly, we confirmed on DESI-MS that these AVA-resistant mice also demonstrated a reduction in anaerobic metabolism, evidenced by a reduction in pyruvate to lactate conversion, after treatment with GLSi therapy. These findings, combined with our up-front evaluation of GLSi therapy discussed above, suggest that GLSi therapy is of value when given in combination or sequentially with AVA.

Therefore, GLSi therapy may prove to be beneficial in the clinical realm for patients whose disease relapses after exposure to AVA or is AVA-resistant.

Assessment of therapeutic efficacy in real-time using HP-MRS

In addition to prospectively evaluating the efficacy of GLSi therapy in these mouse models, we also sought to assess the therapeutic efficacy in real-time with HP-MRS. This technology has been studied in multiple solid tumors as a novel method of assessing treatment response in a manner that was previously inaccessible to imaging.⁶⁶ As it stands, demonstrating a treatment effect of either standard or experimental treatments in patients with ovarian cancer is limited to imaging studies such as computerized tomography (CT) or magnetic resonance imaging (MRI) that are obtained several months after initiating treatment. These techniques are focused on the detection of anatomical changes that occur on a macroscopic level after treatment. Specifically, they use tumor size as a biomarker for treatment response, which often occurs at a slow rate after starting therapy.⁷⁰ Moreover, CT and MRI lack the ability to assess the functional alterations that occur within the tumor prior to any changes in tumor volume that would be apparent on imaging.⁷⁰

In the present study, we utilized HP-MRS to assess therapeutic effect of the GLSi treatment in our *in vivo* models. Using this functional imaging technique, we were able to quantitatively evaluate the flux of pyruvate in the orthotopic tumors after treatment with GLSi, thereby assessing the degree of anaerobic metabolism present within them. We know that higher levels of anaerobic metabolism are associated with more aggressive malignancies and, in essence, the level of pyruvate to lactate

metabolism can serve as a biomarker of treatment response.⁷¹ In our study, we observed that mice treated with GLSi had a reduced conversion of pyruvate to lactate, an early marker of treatment efficacy in this model.

These preliminary studies further emphasize the potential of HP-MRS to be applied in the clinical realm to allow for an assessment of treatment-efficacy in real-time. In doing so, HP-MRS in human patients could allow for identification of treatment response, or a lack thereof, in ovarian cancer. The benefit of HP-MRS utilized for this purpose is that it could be performed at an earlier time point than traditional CT or MRI assessment of macroscopic disease changes. Ultimately, this would allow clinicians to identify a treatment failure sooner and focus their efforts on alternative treatment strategies before the disease progresses even further.

Limitations

Limitations of this study include the utilization of a single ovarian cancer cell line for the *in vivo* investigations. However, the author selected the SKOV3ip1 ovarian cancer cell line due to the expression profile of GLS making it the most suitable candidate for study. Additionally, while the study provided a well-rounded assessment of metabolic adaptations of ovarian cancer cell lines and tumors exposed to hypoxic environments and GLSi treatment, definitive evaluation of the mechanisms of resistance and therapy response(s) were limited and merit further investigation. Furthermore, while we observed a clear relationship between HIF-1 α and GLS expression, the direct linkage between them has not been defined and warrants further study. Lastly, this work did not seek to identify redundant or parallel metabolic pathways at play within the realm of AVA resistance and it is important to

identify these to better understand the impact of targeting GLSi in overcoming AVA resistance.

Study Implications

Over the course of the past decade, ovarian cancer has remained the most lethal gynecologic malignancy, but newer targeted therapies have allowed for a longer survival than has ever been achieved before.⁷² Of these new treatments, AVA therapy with bevacizumab has been a remarkable addition to the armamentarium of options.²⁸ However, the broad adoption of AVA therapy into the treatment schema for both up-front therapy and for recurrent disease also means that there is a growing population of patients that experience adaptive resistance to AVA and are subsequently faced with limited treatment options moving forward.

Here we demonstrated that targeting the glutaminolysis pathway with GLS inhibitor therapy in the AVA-resistant setting is a promising possibility. Although additional studies are needed, we propose that glutaminolysis via the GLS enzyme is a mechanism of resistance in patients treated with AVA therapy and GLSi treatment would be beneficial in this population. Our work suggests that GLSi could be efficacious in combination with AVA therapy up-front or in sequence after AVA therapy is initiated. However, where it may provide the most benefit currently is for the population of patients with recurrent, AVA-resistant disease.

The clinical testing of GLS inhibitors is still in its infancy with only a few trials including women with ovarian cancer and, of those, there has been no direct focus on treatment of AVA-resistant disease specifically. Recently, a phase I clinical trial assessed the effect of a novel GLSi (IACS-6274) in patients with advanced ovarian

cancer and demonstrated a disease control rate of 60% and durable stable disease for at least six months in two patients with ovarian cancer.^{73,74} Within this trial, a biomarker called asparagine synthetase (ASNS) was identified as a useful clinical tool to predict response to GLSi therapy.⁷³ The implications from our current study suggest that the combination of AVA and GLSi treatment may produce enhanced antitumor activity in at least some patients. Perhaps utilization of ASNS as a means of molecular selection for patients to receive therapy could optimize the treatment benefit. Based on the preclinical data generated as a part of this work, there is a triple combination treatment trial with taxane chemotherapy, AVA and GLSi being finalized with the goal to start within six months. This is an exciting development that will also allow for interrogation of tumor samples while patients are on treatment. As these clinical trials mature and progress into phase II and phase III studies, it will be interesting to see the degree and durability of treatment responses.

Future Directions

The next conceptual advance in response to the data presented here requires the development of a phase I clinical trial to test the safety profile and efficacy of GLSi treatment specifically within AVA-resistant ovarian cancer. Toxicity will have to be closely monitored considering our observations from our *in vivo* experiments. It will also be important to carefully examine the response to therapy in these patients in order to better detect biomarkers. Our *in vivo* analysis of therapeutic efficacy by HP-MRS invite further development in this realm as a potential avenue for real-time investigation of treatment response far before it can be detected on CT or MRI imaging.

CONCLUSIONS

In the present study, we identified ubiquitous expression of GLS in ovarian cancer cell lines and confirmed that treatment with AVA (bevacizumab) is associated with an upregulation of GLS as a metabolic adaptation occurring in both cancer cells and in endothelial cells where AVA functions. This upregulation occurs in an HIF-1 α dependent fashion in both cell types and we targeted this hypoxia-mediated increase in GLS expression using GLSi therapy. *In vitro*, we observed significant vulnerability of bevacizumab-resistant RF24 cells (RF24-Bev) to this therapy and noted a profound antitumor effect of GLSi in the SKOV3ip1 ovarian cancer orthotopic mouse model of adaptive resistance to AVA. Of note, we demonstrated efficacy of GLSi when given together with AVA as up-front therapy and when added to AVA after the emergence of resistance. Our *in vivo* studies suggest that this combination therapy is well tolerated.

In sum, we showed that GLSi therapy, when combined with AVA treatment, has robust antitumor effects in preclinical models. This combined therapy warrants further investigations evaluating biologic markers that could predict response of ovarian cancer to GLSi therapy. In addition, future studies evaluating the combination of GLSi with additional chemotherapy drugs are warranted. Our findings provide hope of expanding the utility and efficacy of AVA in the clinical treatment of ovarian cancer, particularly in the AVA-resistant setting.

BIBLIOGRAPHY

1. Cancer Stat Facts: Ovarian Cancer. SEER Research Data 2011-2017 Web site. <https://seer.cancer.gov/data/citation.html>. Published 2022. Accessed March 8, 2022.
2. Al Tameemi W, Dale TP, Al-Jumaily RMK, Forsyth NR. Hypoxia-Modified Cancer Cell Metabolism. *Frontiers in cell and developmental biology*. 2019;7:4-4.
3. Gyorffy B, Lánczky A, Szállási Z. Implementing an online tool for genome-wide validation of survival-associated biomarkers in ovarian-cancer using microarray data from 1287 patients. *Endocr Relat Cancer*. 2012;19(2):197-208.
4. Torre LA, Trabert B, DeSantis CE, Miller KD, Samimi G, Runowicz CD, Gaudet MM, Jemal A, Siegel RL. Ovarian cancer statistics, 2018. *CA Cancer J Clin*. 2018;68(4):284-296.
5. Society AC. Signs and Symptoms of Ovarian Cancer. 2018.
6. Ledermann JA, Raja FA, Fotopoulou C, Gonzalez-Martin A, Colombo N, Sessa C. Newly diagnosed and relapsed epithelial ovarian carcinoma: ESMO Clinical Practice Guidelines for diagnosis, treatment and follow-up. *Ann Oncol*. 2018;29(Supplement_4):iv259-iv259.
7. Chase DM, Neighbors J, Perhanidis J, Monk BJ. Gastrointestinal symptoms and diagnosis preceding ovarian cancer diagnosis: Effects on treatment allocation and potential diagnostic delay. *Gynecol Oncol*. 2021;161(3):832-837.

8. Evans J, Ziebland S, McPherson A. Minimizing delays in ovarian cancer diagnosis: an expansion of Andersen's model of 'total patient delay'. *Fam Pract.* 2006;24(1):48-55.
9. Seltzer V, Batson JL, Drukker BH, Gillespie BW, Gossfeld LM, Grigsby PW, Harvey HA, Hendricks CB, Hummel S, Makuch RW, Monaco GP, Parham GP, Sawyers CL, West RJ. Ovarian-Cancer - Screening, Treatment, and Follow-Up. *Jama-Journal of the American Medical Association.* 1995;273(6):491-497.
10. Langerak AD. Chemotherapeutic Drug Toxicities and Mechanisms of Action. In: CRC Press; 2001:193-210.
11. Sandercock J, Parmar MKB, Torri V, Qian W. First-line treatment for advanced ovarian cancer: paclitaxel, platinum and the evidence. *Br J Cancer.* 2002;87(8):815-824.
12. Herzog TJ, Pothuri B. Ovarian cancer: a focus on management of recurrent disease. *Nature clinical practice Oncology.* 2006;3(11):604-611.
13. Kemp Z, Ledermann J. Update on first-line treatment of advanced ovarian carcinoma. *International journal of women's health.* 2013;5(default):45-51.
14. F.D.A. Avastin (bevacizumab) Information U.S. Food & Drug Administration. Postmarket Drug Safety Information for Patients and Providers Web site. Published 2018. Updated 02/05/2018. Accessed 12/4, 2020.
15. Jain RK. Antiangiogenesis strategies revisited: from starving tumors to alleviating hypoxia. *Cancer Cell.* 2014;26(5):605-622.
16. Hanahan D. Hallmarks of Cancer: New Dimensions. *Cancer Discov.* 2022;12(1):31-46.

17. Ferrara N, Hillan KJ, Gerber H-P, Novotny W. Discovery and development of bevacizumab, an anti-VEGF antibody for treating cancer. *Nature reviews Drug discovery*. 2004;3(5):391-400.
18. Mahdi A, Darvishi B, Majidzadeh-A K, Salehi M, Farahmand L. Challenges facing antiangiogenesis therapy: The significant role of hypoxia-inducible factor and MET in development of resistance to anti-vascular endothelial growth factor-targeted therapies. *J Cell Physiol*. 2019;234(5):5655-5663.
19. Bailey-Serres J, Fukao T, Gibbs DJ, Holdsworth MJ, Lee SC, Licausi F, Perata P, Voeselek LACJ, van Dongen JT. Making sense of low oxygen sensing. *Trends in plant science*. 2012;17(3):129-138.
20. Koh MY, Powis G. Passing the baton: the HIF switch. *Trends Biochem Sci*. 2012;37(9):364-372.
21. Fleet A. Radiobiology for the Radiologist: 6th edition, Eric J. Hall, Amato J. Giaccia, Lippincott Williams and Wilkins Publishing; ISBN 0-7817-4151-3; 656 pages; 2006; Hardback; £53. *Journal of Radiotherapy in Practice*. 2006;5(4):237-237.
22. Hanahan D, Weinberg RA. Hallmarks of cancer: the next generation. *Cell*. 2011;144(5):646-674.
23. McIntyre A, Harris AL. Metabolic and hypoxic adaptation to anti-angiogenic therapy: a target for induced essentiality. *EMBO Mol Med*. 2015;7(4):368-379.
24. Haunschild CE, Tewari KS. Bevacizumab use in the frontline, maintenance and recurrent settings for ovarian cancer. *Future Oncol*. 2019;16(7):225-246.

25. Aghajanian C, Blank SV, Goff BA, Judson PL, Teneriello MG, Husain A, Sovak MA, Jing YI, Nycum LR. OCEANS: A Randomized, Double-Blind, Placebo-Controlled Phase III Trial of Chemotherapy With or Without Bevacizumab in Patients With Platinum-Sensitive Recurrent Epithelial Ovarian, Primary Peritoneal, or Fallopian Tube Cancer. *J Clin Oncol*. 2012;30(17):2039-2045.
26. Perren TJ, Swart AM, Pfisterer J, Ledermann JA, Pujade-Lauraine E, Kristensen G, Carey MS, Beale P, Cervantes A, Kurzeder C, du Bois A, Sehouli J, Kimmig R, Stahle A, Collinson F, Essapen S, Gourley C, Lortholary A, Selle F, Mirza MR, Leminen A, Plante M, Stark D, Qian W, Parmar MK, Oza AM, Investigators I. A phase 3 trial of bevacizumab in ovarian cancer. *N Engl J Med*. 2011;365(26):2484-2496.
27. Pujade-Lauraine E, Hilpert F, Pereira D, Wimberger P, Oaknin A, Mirza MR, Follana P, Bollag D, Ray-Coquard I, Weber B, Reuss A, Poveda A, Kristensen G, Sorio R, Vergote I, Witteveen P, Bamias A. Bevacizumab Combined With Chemotherapy for Platinum-Resistant Recurrent Ovarian Cancer: The AURELIA Open-Label Randomized Phase III Trial. *J Clin Oncol*. 2014;32(13):1302-1308.
28. Burger RA, Brady MF, Bookman MA, Fleming GF, Monk BJ, Huang H, Mannel RS, Homesley HD, Fowler J, Greer BE, Boente M, Birrer MJ, Liang SX. Incorporation of Bevacizumab in the Primary Treatment of Ovarian Cancer. *The New England journal of medicine*. 2011;365(26):2473-2483.

29. Pisarsky L, Bill R, Fagiani E, Dimeloe S, Goosen RW, Hagmann J, Hess C, Christofori G. Targeting Metabolic Symbiosis to Overcome Resistance to Anti-angiogenic Therapy. *Cell Rep.* 2016;15(6):1161-1174.
30. Broglio KR, Berry DA. Detecting an Overall Survival Benefit that Is Derived From Progression-Free Survival. *JNCI : Journal of the National Cancer Institute.* 2009;101(23):1642-1649.
31. Xia Y, Choi H-K, Lee K. Recent advances in hypoxia-inducible factor (HIF)-1 inhibitors. *Eur J Med Chem.* 2012;49:24-40.
32. Warburg O. On the Origin of Cancer Cells. *Science (American Association for the Advancement of Science).* 1956;123(3191):309-314.
33. Liberti MV, Locasale JW. The Warburg Effect: How Does it Benefit Cancer Cells? *Trends in biochemical sciences (Amsterdam Regular ed).* 2016;41(3):211-218.
34. Altman BJ, Stine ZE, Dang CV. From Krebs to clinic: glutamine metabolism to cancer therapy. *Nature reviews Cancer.* 2016;16(10):619-634.
35. Masisi BK, El Ansari R, Alfarsi L, Rakha EA, Green AR, Craze ML. The role of glutaminase in cancer. *Histopathology.* 2020;76(4):498-508.
36. Fuchs BC, Bode BP. Stressing Out Over Survival: Glutamine as an Apoptotic Modulator. *The Journal of surgical research.* 2006;131(1):26-40.
37. Wise DR, Thompson CB. Glutamine addiction: a new therapeutic target in cancer. *Trends Biochem Sci.* 2010;35(8):427-433.
38. Yang L, Moss T, Mangala LS, Marini J, Zhao H, Wahlig S, Armaiz-Pena G, Jiang D, Achreja A, Win J, Roopaimoole R, Rodriguez-Aguayo C, Mercado-Uribe I, Lopez-Berestein G, Liu J, Tsukamoto T, Sood AK, Ram PT, Nagrath

- D. Metabolic shifts toward glutamine regulate tumor growth, invasion and bioenergetics in ovarian cancer. *Mol Syst Biol.* 2014;10(5):728.
39. Moreadith RW, Lehninger AL. The pathways of glutamate and glutamine oxidation by tumor cell mitochondria. Role of mitochondrial NAD(P)⁺-dependent malic enzyme. *The Journal of biological chemistry.* 1984;259(10):6215-6221.
40. Katt WP, Lukey MJ, Cerione RA. A tale of two glutaminases: homologous enzymes with distinct roles in tumorigenesis. *Future Med Chem.* 2017;9(2):223-243.
41. Le A, Lane Andrew N, Hamaker M, Bose S, Gouw A, Barbi J, Tsukamoto T, Rojas Camilio J, Slusher Barbara S, Zhang H, Zimmerman Lisa J, Liebler Daniel C, Slebos Robbert JC, Lorkiewicz Pawel K, Higashi Richard M, Fan Teresa WM, Dang Chi V. Glucose-Independent Glutamine Metabolism via TCA Cycling for Proliferation and Survival in B Cells. *Cell Metab.* 2012;15(1):110-121.
42. Selleckchem.com. Telaglenastat (CB-839).
<https://www.selleckchem.com/products/cb-839.html>. Published 2022.
Accessed.
43. Gross MI, Demo SD, Dennison JB, Chen L, Chernov-Rogan T, Goyal B, Janes JR, Laidig GJ, Lewis ER, Li J, MacKinnon AL, Parlanti F, Rodriguez MLM, Shwonek PJ, Sjogren EB, Stanton TF, Wang T, Yang J, Zhao F, Bennett MK. Antitumor Activity of the Glutaminase Inhibitor CB-839 in Triple-Negative Breast Cancer. *Mol Cancer Ther.* 2014;13(4):890-901.

44. Study of the Glutaminase Inhibitor CB-839 in Solid Tumors. In:February 17, 2020.
45. KEAPSAKE: A Study of Telaglenastat (CB-839) With Standard-of-Care Chemoimmunotherapy in 1L KEAP1/NRF2-Mutated, Nonsquamous NSCLC. In:November 9, 2021.
46. CB-839 HCl in Combination With Carfilzomib and Dexamethasone in Treating Patients With Recurrent or Refractory Multiple Myeloma. In:August 26, 2021.
47. Study of CB-839 (Telaglenastat) in Combination With Talazoparib in Patients With Solid Tumors. In:August 18, 2021.
48. A Study of Telaglenastat (CB-839) in Combination With Palbociclib in Patients With Solid Tumors. In:October 29, 2021.
49. Wu C, Chen L, Jin S, Li H. Glutaminase inhibitors: a patent review. *Expert Opin Ther Pat.* 2018;28(11):823-835.
50. A Comparative, Pharmacokinetic Study of CB-839 Capsule and Tablet Formulations in Healthy Adults. In:January 4, 2017.
51. Study of CB-839 in Combination w/ Paclitaxel in Patients of African Ancestry and Non-African Ancestry With Advanced Triple Negative Breast Cancer (TNBC). In:August 19, 2021.
52. Testing of the Anti Cancer Drugs CB-839 HCl (Telaglenastat) and MLN0128 (Sapanisertib) in Advanced Stage Non-small Cell Lung Cancer. In:October 1, 2021.
53. CANTATA: CB-839 With Cabozantinib vs. Cabozantinib With Placebo in Patients With Metastatic Renal Cell Carcinoma. In:August 23, 2021.

54. CB-839 in Combination With Niraparib in Platinum Resistant BRCA -Wild-type Ovarian Cancer Patients. In:October 21, 2021.
55. ENTRATA: CB-839 With Everolimus vs. Placebo With Everolimus in Patients With Renal Cell Carcinoma (RCC). In.
56. Hudson CD, Savadelis A, Nagaraj AB, Joseph P, Avril S, DiFeo A, Avril N. Altered glutamine metabolism in platinum resistant ovarian cancer. *Oncotarget*. 2016;7(27):41637-41649.
57. Masamha CP, LaFontaine P. Molecular targeting of glutaminase sensitizes ovarian cancer cells to chemotherapy. *J Cell Biochem*. 2018;119(7):6136-6145.
58. Livak KJ, Schmittgen TD. Analysis of relative gene expression data using real-time quantitative PCR and the 2(T)(-Delta Delta C) method. *Methods*. 2001;25(4):402-408.
59. Landen CN, Chavez-Reyes A, Bucana C, Schmandt R, Deavers MT, Lopez-Berestein G, Sood AK. Therapeutic EphA2 gene targeting in vivo using neutral liposomal small interfering RNA delivery. *Cancer research (Chicago, Ill)*. 2005;65(15):6910-6918.
60. Zhou W, Yao Y, Scott AJ, Wilder-Romans K, Dresser JJ, Werner CK, Sun H, Pratt D, Sajjakulnukit P, Zhao SG, Davis M, Nelson BS, Halbrook CJ, Zhang L, Gatto F, Umemura Y, Walker AK, Kachman M, Sarkaria JN, Xiong J, Morgan MA, Rehemtualla A, Castro MG, Lowenstein P, Chandrasekaran S, Lawrence TS, Lyssiotis CA, Wahl DR. Purine metabolism regulates DNA repair and therapy resistance in glioblastoma. *Nat Commun*. 2020;11(1):3811.

61. Tusher VG, Tibshirani R, Chu G. Significance Analysis of Microarrays Applied to the Ionizing Radiation Response. *Proceedings of the National Academy of Sciences - PNAS*. 2001;98(9):5116-5121.
62. Wiseman JM, Ifa DR, Song Q, Cooks RG. Tissue Imaging at Atmospheric Pressure Using Desorption Electrospray Ionization (DESI) Mass Spectrometry. *Angewandte Chemie*. 2006;118(43):7346-7350.
63. Eberlin LS, Ferreira CR, Dill AL, Ifa DR, Cheng L, Cooks RG. Nondestructive, Histologically Compatible Tissue Imaging by Desorption Electrospray Ionization Mass Spectrometry. *Chembiochem : a European journal of chemical biology*. 2011;12(14):2129-2132.
64. Xiang L, Mou J, Shao B, Wei Y, Liang H, Takano N, Semenza GL, Xie G. Glutaminase 1 expression in colorectal cancer cells is induced by hypoxia and required for tumor growth, invasion, and metastatic colonization. *Cell Death Dis*. 2019;10(2):40.
65. Buffa FM, Harris AL, West CM, Miller CJ. Large meta-analysis of multiple cancers reveals a common, compact and highly prognostic hypoxia metagene. *Br J Cancer*. 2010;102(2):428-435.
66. Wang ZJ, Ohliger MA, Larson PEZ, Gordon JW, Bok RA, Slater J, Villanueva-Meyer JE, Hess CP, Kurhanewicz J, Vigneron DB. Hyperpolarized C-13 MRI: State of the Art and Future Directions. *Radiology*. 2019;291(2):273-284.
67. Cluntun AA, Lukey MJ, Cerione RA, Locasale JW. Glutamine Metabolism in Cancer: Understanding the Heterogeneity. *Trends in cancer*. 2017;3(3):169-180.

68. Yang L, Achreja A, Yeung TL, Mangala LS, Jiang D, Han C, Baddour J, Marini JC, Ni J, Nakahara R, Wahlig S, Chiba L, Kim SH, Morse J, Pradeep S, Nagaraja AS, Haemmerle M, Kyunghee N, Derichsweiler M, Plackemeier T, Mercado-Uribe I, Lopez-Berestein G, Moss T, Ram PT, Liu J, Lu X, Mok SC, Sood AK, Nagrath D. Targeting Stromal Glutamine Synthetase in Tumors Disrupts Tumor Microenvironment-Regulated Cancer Cell Growth. *Cell Metab.* 2016;24(5):685-700.
69. Cory JG, Cory AH. Critical Roles of Glutamine as Nitrogen Donors in Purine and Pyrimidine Nucleotide Synthesis: Asparaginase Treatment in Childhood Acute Lymphoblastic Leukemia. *In vivo (Athens).* 2006;20(5):587-589.
70. Kyriazi S, Kaye SB, deSouza NM. Imaging ovarian cancer and peritoneal metastases-current and emerging techniques. *Nature reviews Clinical oncology.* 2010;7(7):381-393.
71. Dutta P, Castro Pando S, Mascaro M, Riquelme E, Zoltan M, Zacharias NM, Gammon ST, Piwnica-Worms D, Pagel MD, Sen S, Maitra A, Shams S, McAllister F, Bhattacharya PK. Early Detection of Pancreatic Intraepithelial Neoplasias (PanINs) in Transgenic Mouse Model by Hyperpolarized ¹³C Metabolic Magnetic Resonance Spectroscopy. *Int J Mol Sci.* 2020;21(10):3722.
72. Lim HJ, Ledger W. Targeted therapy in ovarian cancer. *Women's health (London, England).* 2016;12(3):363-378.
73. Yap TA, Dumbrava EE, Ahnert JR, Hong DS, Pant S, Karp DD, Piha-Paul SAA, Subbiah V, Tsimberidou AM, Fu SQ, Janku F, Montez S, Ahmad-Taha MT, Guerrero D, Nazarenko NN, Moore Y, Soth M, Kovacs J, Heffernan TP,

- Jones P. First-in-human biomarker-driven phase I trial of the potent and selective glutaminase-1 (GLS1) inhibitor IACS-6274 (IPN60090) in patients (pts) with molecularly selected advanced solid tumors. *J Clin Oncol.* 2021;39(15):3001-3001.
74. Oncology - Solid Cancer; A Phase I, Open Label, Dose Escalation and Dose Expansion Study to Investigate the Safety, Pharmacokinetics, Pharmacodynamics and Anti-tumour Activity of IPN60090 as Single Agent and in Combination in Patients With Advanced Solid Tumours. *Clinical trials week.* 2019:114.

Permissions

For Figure 2:

License Number

5287120912026

License date

Apr 13, 2022

Licensed Content Publisher

John Wiley and Sons

Licensed Content Publication

Journal of Cellular Physiology

Licensed Content Title

Challenges facing antiangiogenesis therapy: The significant role of hypoxia-inducible factor and MET in development of resistance to anti-vascular endothelial growth factor-targeted therapies

Licensed Content Author

Leila Farahmand, Malihe Salehi, Keivan Majidzadeh-A, et al

Licensed Content Date

Dec 4, 2018

Licensed Content Volume

234

Licensed Content Issue

5

Licensed Content Pages

9

Type of use

Dissertation/Thesis

Requestor type

University/Academic

Format

Print

Portion

Figure/table

Number of figures/tables

1

Will you be translating?

No

Title

MD

Institution name

MD Anderson Cancer Center

Expected presentation date

Apr 2022

Portions

Figure 1 on page 5657

For Figure 4 (Left):

License Number

5287140658961

License date

Apr 13, 2022

Licensed Content Publisher

Wolters Kluwer Health, Inc.

Licensed Content Publication

Journal of Clinical Oncology

Licensed Content Title

Bevacizumab Combined With Chemotherapy for Platinum-Resistant Recurrent Ovarian Cancer: The AURELIA Open-Label Randomized Phase III Trial

Licensed Content Author

Eric Pujade-Lauraine, Felix Hilpert, Béatrice Weber, et al

Licensed Content Date

May 1, 2014

Licensed Content Volume

32

Licensed Content Issue

13

Type of Use

Dissertation/Thesis

Requestor type

University/College

Sponsorship

No Sponsorship

Format

Print

Portion

Figures/tables/illustrations

Number of figures/tables/illustrations

1

Author of this Wolters Kluwer article

No

Will you be translating?

No

Portions

Figure 2, PFS

For Figure 4 (Right):

License Number

5287140958721

License date

Apr 13, 2022

Licensed Content Publisher

Wolters Kluwer Health, Inc.

Licensed Content Publication

Journal of Clinical Oncology

Licensed Content Title

OCEANS: A Randomized, Double-Blind, Placebo-Controlled Phase III Trial of Chemotherapy With or Without Bevacizumab in Patients With Platinum-Sensitive Recurrent Epithelial Ovarian, Primary Peritoneal, or Fallopian Tube Cancer

Licensed Content Author

Carol Aghajanian, Stephanie V. Blank, Barbara A. Goff, et al

Licensed Content Date

Jun 10, 2012

Licensed Content Volume

30

Licensed Content Issue

17

Type of Use

Dissertation/Thesis

Requestor type

University/College

Sponsorship

No Sponsorship

Format

Print

Portion

Figures/tables/illustrations

Number of figures/tables/illustrations

1

Author of this Wolters Kluwer article

No

Will you be translating?

No

Intend to modify/change the content

No

Title

MD

Institution name

MD Anderson Cancer Center

Expected presentation date

Apr 2022

Portions

Figure 2, PFS

For Figure 5:

License Number

5287141314876

License date

Apr 13, 2022

Licensed Content Publisher

Springer Nature

Licensed Content Publication

Nature Reviews Cancer

Licensed Content Title

From Krebs to clinic: glutamine metabolism to cancer therapy

Licensed Content Author

Brian J. Altman et al

Licensed Content Date

Jul 29, 2016

Type of Use

Thesis/Dissertation

Requestor type

academic/university or research institute

Format

print

Portion

figures/tables/illustrations

Number of figures/tables/illustrations

1

High-res required

no

Will you be translating?

no

Circulation/distribution

30 - 99

Author of this Springer Nature content

no

Title

MD

Institution name

MD Anderson Cancer Center

Expected presentation date

Apr 2022

Portions

Figure 2, page 621

Vita

Deanna Glassman was born in Missoula, Montana, the second of two daughters to Tom and Nancy Malikie. She was raised in Montana and graduated from Valley Christian High School, a private K-12 academic environment. She then moved to Tacoma, Washington where she began her undergraduate studies at the University of Puget Sound. She received a Bachelor of Science in Exercise Science and was recognized as the 2009 Roberta Wilson Outstanding Graduate of the Year. She then spent several years working as a medical scribe in the Emergency Department at Tacoma General Hospital before matriculating at the University of Washington School of Medicine in 2012. She received her medical doctorate in 2016, graduating with Honors from the institution before moving across the United States where she entered the Obstetrics and Gynecology residency program at the Warren Alpert Medical School of Brown University in Providence, Rhode Island. She completed her training in 2020 and then began a fellowship in Gynecologic Oncology at the University of Texas M.D. Anderson Cancer Center. Her two-year Master's program during this fellowship was mentored by Dr. Anil K. Sood and focused on the development of therapeutics to combat adaptive resistance to anti-VEGF antibody therapy.

Permanent Address:
2807 Prescott Street
Houston, TX
77025